Manuscript submitted to
AIMS' Journals
Volume **X**, Number **0X**, XX **200X**

Website: http://AIMsciences.org

pp. **X–XX**

ATTRACTORS FOR RETURN MAPS NEAR HOMOCLINIC TANGENCIES OF THREE-DIMENSIONAL DISSIPATIVE DIFFEOMORPHISMS

Antonio Pumariño

Departamento de Matemáticas, Universidad de Oviedo
Calvo Sotelo s/n, 33.007 Oviedo, Spain

Joan Carles Tatjer

Departament de Matemàtica Aplicada i Anàlisi, Universitat de Barcelona
Gran Via, 585, 08.007 Barcelona, Spain

(Communicated by the associate editor name)

Abstract. We numerically analyse different kinds of one-dimensional and two-dimensional attractors for the limit return map associated to the unfolding of homoclinic tangencies for a large class of three-dimensional dissipative diffeomorphisms. Besides describing the topological properties of these attractors, we often numerically compute their Lyapunov exponents in order to clarify where two-dimensional strange attractors can show up in the parameter space. Hence, we are specially interested in the case in which the unstable manifold of the periodic saddle taking part in the homoclinic tangency has dimension two.

1. **Introduction.** From the time of Poincaré [18] to the present days, the homoclinic phenomena have been extensively studied for parameter families of diffeomorphisms defined in two-dimensional manifolds, see [16] for a complete overview on the subject. In a few words, homoclinic orbits appear when an intersection between the stable and the unstable manifolds of a periodic saddle point takes place, and the first homoclinic orbit (the degenerate homoclinic orbit that firstly appears as parameters are moved), usually called a homoclinic tangency, corresponds to a tangential connection between those invariant manifolds. For the bidimensional case, a great program has been developed in order to describe the intrincate dynamics appearing in the unfolding of a homoclinic tangency. We cite [4], [14] and [15] to recall the complicated dynamical objects (infinitely many sinks, persistent strange attractors and infinitely many strange attractors) which may accompany the unfolding of homoclinic tangencies in the bidimensional setting.

By an attractor for a transformation f defined in a manifold M we mean a compact, f-invariant and transitive set A whose stable set

$$W^s(A) = \{z \in M : d(f^n(z), A) \to 0 \text{ as } n \to \infty\}$$

2000 *Mathematics Subject Classification.* Primary: 37G35; Secondary: 37C29 37D45.

Key words and phrases. Invariant curves, strange attractors, Lyapunov exponents.

This work has been partially supported by MEC grants MTM2005-02094 and FEDER MTM2006-11265, and CIRIT grant 2005SGR01028.

has nonempty interior. An attractor is said to be strange if it contains a dense orbit $\{f^n(z_1) : n \geq 0\}$ displaying exponential growth of the derivative: There exists some positive constant c such that, for every $n \geq 0$,

$$\|Df^n(z_1)\| \geq \exp(cn).$$

We have chosen this definition because it is more convenient from the numerical point of view. Another possibility is to ask for sensitive dependence to initial conditions, but this is difficult to check in computations. In any case, there are different definitions of strange attractors and even of attractors in the literature (see e. g. [12]). The above-mentioned bidimensional results are strongly based on the existence of limit return maps defined in a neighbourhood of the homoclinic orbit for values of the parameter close enough to that one giving rise to the first homoclinic tangency. Since we are specially interested in the unfolding of certain homoclinic tangencies for diffeomorphisms defined in three-dimensional manifolds, let us recover from [24] a general definition of limit return maps. Before that, let us recall that a fixed point p of a diffeomorphism f defined in a manifold of dimension m is said to be dissipative if $|\lambda_1 \cdots \lambda_m| < 1$, where $\lambda_1, \ldots, \lambda_m$ are the eigenvalues of $Df(p)$.

Definition 1.1. Let $\{f_a\}_{a \in V}$ be a smooth family of diffeomorphisms in some m-dimensional manifold M, depending on a parameter $a \in V \subset \mathbb{R}^k$, V being an open subset. Suppose that for $a = a_0$ there exists a homoclinic orbit O_0 of some dissipative fixed point p_0 of f_{a_0}. We say that the family $\{f_a\}_{a \in V}$ has a family of **limit return maps** associated to the homoclinic orbit O_0, in the C^l topology, if there exists a point q of the homoclinic orbit and a natural number N, such that for any positive integer $n \geq N$ there exist reparametrizations $a = M_n(\widetilde{a})$ of the a variable and $\widetilde{a}$-dependent coordinate transformations $x = \Psi_{n,\widetilde{a}}(\widetilde{x})$ satisfying the following properties:

1.- For each compact set K in the $(\widetilde{a}, \widetilde{x})$ space the images of K under the maps

$$(\widetilde{a}, \widetilde{x}) \to (M_n(\widetilde{a}), \Psi_{n,\widetilde{a}}(\widetilde{x}))$$

converge, for $n \to \infty$, in the $(\widetilde{a}, \widetilde{x})$ space, to (a_0, q).

2.- The domains of the maps

$$(\widetilde{a}, \widetilde{x}) \to \left(\widetilde{a}, \left(\Psi^{-1}_{n,\widetilde{a}} \circ f^n_{M_n(\widetilde{a})} \circ \Psi_{n,\widetilde{a}}\right)(\widetilde{x})\right)$$

converge, for $n \to \infty$, to $\mathbb{R}^{m+k}$, and the maps converge, in the C^l topology, to some map of the form

$$(\widetilde{a}, \widetilde{x}) \to \left(\widetilde{a}, \widetilde{f}_{\widetilde{a}}(\widetilde{x})\right).$$

In this case, we say that $\left\{\widetilde{f}_{\widetilde{a}}\right\}_{\widetilde{a} \in \mathbb{R}^k}$ is a family of limit return maps associated to the homoclinic orbit O_0.

The existence of a family $\left\{\widetilde{f}_{\widetilde{a}}\right\}_{\widetilde{a} \in \mathbb{R}^k}$ of limit return maps means that, up to a change of coordinates, the dynamics (in a neighbourhood of some homoclinic point) of a sufficiently large power of f_a looks like the dynamics of some $\widetilde{f}_{\widetilde{a}}$. The main advantage to work with a family of limit return maps is that it is valid for generic situations: The same family of limit return maps "represents" a generic set of families of diffeomorphisms $\{f_a\}_{a \in V}$ having homoclinic tangencies unfolding generically.

For generic one-parameter families of diffeomorphisms on surfaces unfolding a homoclinic tangency, i.e., when $k = 1$ and $m = 2$, it can be shown, see [14] and [16], that the family of "bidimensional" limit return maps $\left\{\widetilde{f}_{\widetilde{a}}\right\}_{\widetilde{a}\in\mathbb{R}}$ is given by

$$\widetilde{f}_{\widetilde{a}}\left(\widetilde{x}_1, \widetilde{x}_2\right) = \left(1 - \widetilde{a}\widetilde{x}_1^2, 0\right). \tag{1}$$

Therefore, these limit return maps essentially behave as the one-dimensional logistic family $Q_a(x) = 1 - ax^2$. Hence, a new advantage arises when a family of limit return maps is obtained: While the original family of diffeomorphisms is defined on a bidimensional space, the family of limit return maps is essentially defined in a one-dimensional domain. As we will see later, this also will be true for our higher dimensional setting: The limit return maps associated to our families of three-dimensional diffeomorphisms will essentially work as two-dimensional endomorphisms. The family given at (1) has played a very important role for understanding not only the dynamics associated to the unfolding of homoclinic tangencies in dimension two, see for instance [14] and [23], but also in other very interesting situations, see [1] and [2].

The same family of limit return maps (1) works for generic one-parameter families of diffeomorphisms defined on an m-dimensional manifold when $\dim\left(W^u\left(p_0\right)\right) = 1$ and p_0 is sectionally dissipative: The eigenvalues $\lambda_1, ..., \lambda_m$ of $Df_{a_0}\left(p_0\right)$ satisfy $|\lambda_1| \leq ... \leq |\lambda_{m-1}| < 1 < |\lambda_m|$ and $|\lambda_{m-1}\lambda_m| < 1$. In the sectionally dissipative case, these limit return maps were already used to prove the coexistence of infinitely many sinks, see [17], and the existence of persistent strange attractors, see [25].

The main goal of the present paper is to numerically explore the dynamics of the family of limit return maps (as expected, they will be noninvertible maps) which "represents" certain two-parameter families ($k = 2$) of three-dimensional diffeomorphisms ($m = 3$) which are dissipative but not sectionally dissipative. In fact, we will put special emphasis in the analogies between the family of limit return maps for the case $m = 2$ (see (1)) and the family of limit return maps for the case $m = 3$ (see (3) below). Furthermore, another aim of the paper is to conjecture (see Conjectures 1 and 2, and Remark 1) that several important results valid in dimension two can be extended to the three dimensional case.

1.1. **The limit return maps for the three dimensional case.** Let us consider a two-parameter family $\{f_{a,b}\}_{a,b}$ of three-dimensional diffeomorphisms having a hyperbolic saddle fixed point p_0 for $(a, b) = (0, 0)$ with real eigenvalues λ_1, λ_2 and λ_3 satisfying the following properties (we refer the reader to [24] for the definition of generalized homoclinic tangency and the statement of the linearization assumption):

1.- The eigenvalues satisfy $0 < |\lambda_1| < 1 < |\lambda_2| < |\lambda_3|$. We remark that from this assumption the corresponding fixed point is never sectionally dissipative.
2.- The invariant manifolds of p_0 have a generalized homoclinic tangency which unfolds generically (we only remark here that in the set of two-parameter families of three-dimensional diffeomorphisms unfolding homoclinic tangencies those ones unfolding a **generalized** homoclinic tangency are generic).
3.- The family $\{f_{a,b}\}_{a,b}$ satisfies the linearization assumption (generic condition for families of diffeomorphisms having saddle fixed points).

In [24] (see Theorem 1) it is proved that the corresponding family of limit return maps is given by

$$\widetilde{f}_{\widetilde{a},\widetilde{b}}\left(\widetilde{x}, \widetilde{y}, \widetilde{z}\right) = \left(\widetilde{z}, \widetilde{a} + \widetilde{b}\widetilde{y} + \widetilde{z}^2, \widetilde{y}\right). \tag{2}$$

Let us point out that, for each $\left(\widetilde{a},\widetilde{b}\right)\in\mathbb{R}^2$, every point in $\mathbb{R}^3$ "falls" by one iteration of the map $\widetilde{f}_{\widetilde{a},\widetilde{b}}$ into the surface

$$C_{\widetilde{a},\widetilde{b}}=\left\{(\widetilde{x},\widetilde{y},\widetilde{z}):\widetilde{y}=\widetilde{a}+\widetilde{b}\widetilde{z}+\widetilde{x}^2\right\}.$$

Hence, $C_{\widetilde{a},\widetilde{b}}$ is invariant by $\widetilde{f}_{\widetilde{a},\widetilde{b}}$ and it is enough to study the dynamics of $\widetilde{f}_{\widetilde{a},\widetilde{b}}$ on $C_{\widetilde{a},\widetilde{b}}$. Using the parameterization of $C_{\widetilde{a},\widetilde{b}}$ given by $P\left(\widetilde{x},\widetilde{z}\right)=\left(\widetilde{x},\widetilde{a}+\widetilde{b}\widetilde{z}+\widetilde{x}^2,\widetilde{z}\right)$, in order to study the behaviour of $\widetilde{f}_{\widetilde{a},\widetilde{b}}$ on $C_{\widetilde{a},\widetilde{b}}$ it suffices, as we said before, to consider the family of bidimensional endomorphisms defined on $\mathbb{R}^2$ by

$$\left(P^{-1}\circ\widetilde{f}_{\widetilde{a},\widetilde{b}}\circ P\right)(\widetilde{x},\widetilde{z})=\left(\widetilde{z},\widetilde{a}+\widetilde{b}\widetilde{z}+\widetilde{x}^2\right).$$

Let us take the change of coordinates $x=\widetilde{z}-\widetilde{b}\widetilde{x}$, $y=\widetilde{x}$ in order to write the above family of transformations in the following way

$$T_{a,b}\left(x,y\right)=\left(a+y^2,x+by\right), \tag{3}$$

where we have written, in order to avoid excessive notation, $a=\widetilde{a}$ and $b=\widetilde{b}$.

For the sake of completeness, we refer the reader to [7], [21] and [24] where the families of return maps for different situations in the three-dimensional framework are given. In any case, we want to stress that the other two families appearing in those papers are related to the not sectionally dissipative cases for which the dimension of the unstable manifold of the saddle point involved in the homoclinic tangency is equal to one. Since we are specially interested in finding **two-dimensional** strange attractors we will restrict our numerical analyses to (3).

Finally, we want to recall that one of the objectives of this paper is to extend the numerical study of the family (3) previously furnished in [21], where we had mainly focussed our attention in the analytical results. In this sense, this paper is organized as follows: In Section 2 we describe the curve in the space of parameters where our numerical experiments are done. This curve of parameters is denoted by G, see (4), and it is contained in the subset of the parameter space for which the map $T_{a,b}$ has an invariant region $R_{a,b}$. The curve G ends at $(a,b)=(-4,-2)$. This special value of the parameter corresponds to the case for which $T_{-4,-2}(R_{-4,-2})$ coincides with $R_{-4,-2}$. As in the well-studied bidimensional case (i.e., when $m=2$) the final value of the parameter, i.e. $(a,b)=(-4,-2)$, becomes very relevant and it is interesting to pay attention to the resemblances of our "final" map $T_{-4,-2}$ and the one-dimensional quadratic map $Q_2(x)=1-2x^2$, which is the Misiurewicz "final" map of the family of limit return maps associated to the unfolding of homoclinic tangencies in the two dimensional framework. Since the dynamical behaviour of the quadratic family dramatically changes when the parameter crosses this final value $a=2$ (recall, for instance, that all the results in [1], [8] and [14], have to be posed for sets of values of the parameter smaller than this final value) the same can be expected for our bidimensional setting. For a more extensive study of the nice properties of our "bidimensional tent map" $T_{-4,-2}$ we again refer the reader to [21]. In Section 3 we introduce our numerical analyses to show the richness of the one-dimensional and two-dimensional attractors exhibited by the family (3) for several values of the parameter (a,b) in G. Finally, in Section 4 we give a brief overview on the behaviour of the whole family $T_{a,b}$, and Section 5 is devoted to summarize the resemblances between the families $T_{a,b}$ and Q_a.

2. **The curve of parameters.** As we said in the Introduction, we look for a region in the set of parameters (a,b) for which our transformation $T_{a,b}$, see (3), has an invariant region and therefore an attractor. This can be easily obtained by taking the parameters in a suitable subset of the line $b=0$. Of course, since $T_{a,0}(x,y)=\left(a+y^2,x\right)$ and $T_{a,0}^2(x,y)=\left(a+x^2,a+y^2\right)$ it follows that $T_{a,0}(R_a)=R_a$ for any $a\in[-2,-1]$, where $R_a=\left[a,a+a^2\right]\times\left[a,a+a^2\right]$. With respect to this special region of the parameters, in [21] it is proved the following result stating the one-dimensional persistence of two-dimensional strange attractors:

Proposition 1. *For any $0<c<\log 2$ there exists $a_0>-2$ and a positive Lebesgue measure set E of values of the parameter a contained in $[-2,a_0]$ such that for any $a\in E$ there exists a dense orbit $\bigcup_{n\in\mathbb{N}}\left\{T_{a,0}^n(x_0,y_0)\right\}$ in R_a and a natural number n_0 such that*

$$\left\|DT_{a,0}^n(x_0,y_0)\,\mathbf{v}\right\|\geq\exp\left(\frac{cn}{2}\right)$$

for any unit vector $\mathbf{v}$ and $n\geq n_0$.

Let us observe that there exist invariant lines for $T_{a,0}^2$. Hence, we have found a fruitful method to get more values of the parameter (a,b) for which the respective map $T_{a,b}$ has an invariant domain: Just to look inside the set of parameters for which $T_{a,b}^2$ has invariant lines. Besides the case $b=0$, it can be shown that this fact happens when one takes a parameter in the curve G given by

$$G=\left\{(a(t),b(t))=\left(-\frac{1}{4}t^3\left(t^3-2t^2+2t-2\right),-t^2+t\right):t\in\mathbb{R}\right\}\tag{4}$$

being the respective invariant line for $T_{a,b}^2$ the one giving by

$$L^1=L^1(t)=\left\{(x,y)\in\mathbb{R}^2:x=A+By;A=\frac{1}{2}\left(t-t^2\right)t^2,\,B=t^2\right\}.\tag{5}$$

Invariant lines also arise when $b=-2$. In this case, the line $x=-1+y$ is invariant for $T_{a,-2}^2$, for all real a. There are no more cases of values of the parameters with invariant lines for $T_{a,b}^2$. It is not difficult to prove that for $b=-2$ and $-2<a<-7/4$ there exists a heteroclinic connection between two saddle two-periodic points, formed by a segment in the line $x=-1+y$ and an arc in the parabola $x=a+(1+y)^2$. For $a\leq-2$ the map $T_{a,-2}$, restricted to the segment in the line and the arc in the parabola forming the border of an open and bounded region, is not invertible. This means that the heteroclinic connection disappears.

Of course, by searching those parameters for which the map $T_{a,b}^2$ has an invariant line, we are not finding all the parameters for which the map $T_{a,b}$ has some invariant region (observe that this last set of parameters must have nonempty interior). Nevertheless, for our numerical purposes, we will restrict our study to those parameters laying in (4). In any case, we think that the dynamical richness exhibited for those parameters belonging to (4) will be enough to realize the great complexity arising in families of dissipative three-dimensional diffeomorphisms unfolding a homoclinic tangency associated to a saddle point whose unstable invariant manifold has dimension two.

Before going on, we introduce Figure 2, where we numerically compute a region $B\subset\mathbb{R}^2$ of the parameter space for which the map $T_{a,b}$ has an invariant domain. Moreover, we also distinguish between four subdomains according to the following criterion: Parameters for which the attractor reduces to a periodic point (the region in pale grey or blue in the electronic version of the paper); parameters for which one

attractor presents a zero Lyapunov exponent and therefore we expect the attractor becomes a finite union of closed curves (the region in intermediate grey or green in the electronic version). Let us observe that these two regions are clearly separated by a segment which matches with a Hopf bifurcation line (see Figure 2). It is easy to check that this bifurcation line is given by the equation $2b-4a=3$, for $-2<b<2$. Indeed, if (x,y) is a fixed point for which there is a Hopf bifurcation, we have that

$$a+y^2=x, \qquad x+by=y, \qquad \det DT_{a,b}(x,y)=-2y=1.$$

Moreover, if we impose the condition that $DT_{a,b}(x,y)$ has non-real eigenvalues, then $[\operatorname{tr} DT_{a,b}(x,y)]^2-4\det DT_{a,b}(x,y)<0$. All these conditions give the desired result. Morever, the two endpoints of this Hopf bifurcation line correspond to codimension-two bifurcations. For $b=2$, the bifurcation line ends at a Bogdanov-Takens bifurcation parameter (1:1 resonance), i.e., $(a,b)=\left(\frac{1}{4},2\right)$, and for $b=-2$ it ends at a bifurcation for which the two eigenvalues of the respective fixed point are equal to -1 (1:2 resonance). We can also compute the value t^* of the parameter t for which the curve G cuts the Hopf bifurcation line as a real zero of the polynomial

$$P(t)=t^6-2t^5+2t^4-2t^3-2t^2+2t-3.$$

We have that $t^*=1.810535713766\ldots$. The region in dark grey (or red in the electronic version of the paper) corresponds to values of the parameter for which the sum and the product of the two Lyapunov exponents of an attractor is negative (one-dimensional strange attractors) and finally, the region in black represents those parameters for which the sum of the Lyapunov exponents of an attractor is positive (two-dimensional strange attractors). Here we follow the usual definition of the Lyapunov dimension, see for instance [9]. Furthermore, the white curve drawn in Figure 2 corresponds to the curve G given in (4) for values of t in $[0,2]$. Outside this range of t there is no interesting phenomenon for $T_{a(t),b(t)}$: Either there is no invariant region, or the attractor reduces to a fixed point. This curve G ends at the point $(-4,-2)$, i.e. $t=2$. Later, we will describe a few properties for the respective map $T_{-4,-2}$, but for a more extensive study of this map we refer the reader to [21]. Another interesting parameter in the boundary of the domain given in Figure 2 is $(-2,0)$, which is a Misiurewicz parameter for the one-parameter family introduced in Proposition 1.

Let us give a brief explanation of how Figure 2 has been obtained. For each value of (a,b) in the set

$$\mathcal{P}=\{(-4+i\Delta a,-2.2+j\Delta b),\ 1\le i,j\le 1000\},\quad \Delta a=4.4\times10^{-3},\quad \Delta b=4.2\times10^{-3}$$

we compute the orbit of two hundred equidistant initial points in the segment

$$\mathcal{V}=\left\{(x,y)\in\mathbb{R}^2 : x\in(-10,10)\,,\ y=0\right\}.$$

Let us observe that the above segment $\mathcal{V}$ is contained in the critical set $y=0$ of our transformation $T_{a,b}$. If the sum of the absolute values of the two components of the first $n=10^6$ iterates of one of these initial points are less than a large number (we have taken 10^{10}), we select the parameter as one for which there exists an invariant domain and compute the Lyapunov exponents along this piece of orbit. We must say that we are not taking into account the possible coexistence of several attractors for the same value of the parameter and, of course, this could imply slight changes in the distribution of the four subdomains depicted in Figure 2, depending on the orbits that one calculates. Overall, in order to find the maximum amount of parameters for which there are invariant domains, once we have decided that

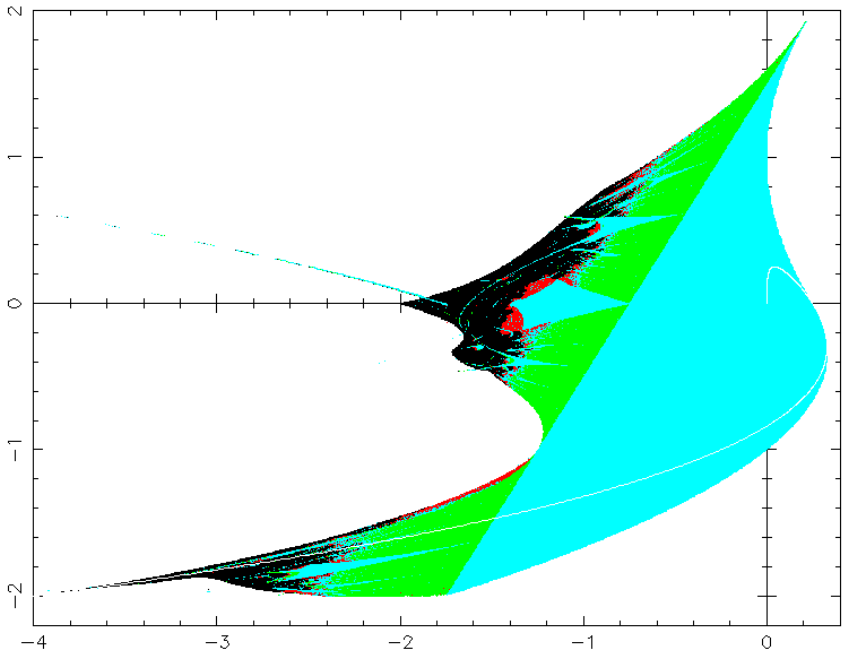

FIGURE 1. Region of parameters a, b for which there are attractors.

a parameter $(a_0, b_0) \in \mathcal{P}$ belongs to the region B for which there are invariant domains, we take the initial point whose orbit remains in the invariant domain, and check if its orbit is bounded for the next tested value of (a, b), i.e. $(a_0, b_0 + \Delta b)$ or $(a_0 + \Delta a, -2.2)$. Moreover, we also do the same with the orbit of the nearest value of (a, b) in the border of the part of B previously computed. It remains as an open question if it is enough to pursue the orbits of critical points in order to ensure the existence of invariant domains, see also Remark 1.

Now we restrict ourselves again to the curve of parameters G. The two fixed points of $T_{a,b}$ are

$$P_{a,b} = ((1-b)y_+, y_+), \qquad \tilde{P}_{a,b} = ((1-b)y_-, y_-), \tag{6}$$

where

$$y_\pm = \frac{1-b \pm \sqrt{(b-1)^2 - 4a}}{2}.$$

The invariant line L^1, see (5), contains the fixed point $P_{a,b}$.

For every t, let us denote by $C_1 = C_1(t)$ the segment of L^1 joining $P_{a,b}$ with the point $L = (A, 0)$, see (5) for the definition of $A = A(t)$. One can show that, taking the parabola

$$L^2 = L^2(t) = \left\{ (x, y) \in \mathbb{R}^2 : x = \left(\frac{y - A}{b + B} \right)^2 + a \right\},$$

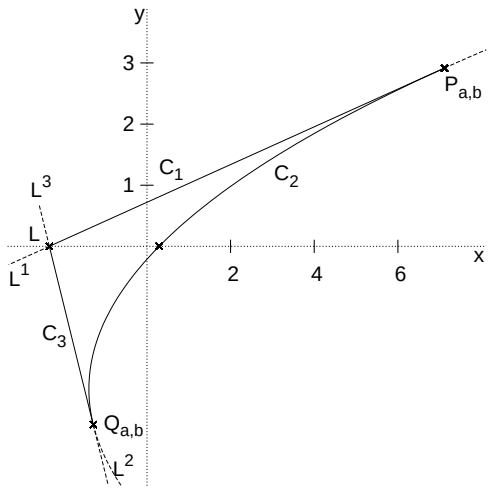

FIGURE 2. The shape of R_t, for $t = 1.8$.

then L^2 contains $P_{a,b}$ and $T_{a,b}(C_1) \subset L^2$. On the other hand, if $Q_{a,b} = Q_{a,b}(t)$ is the unique point different from $P_{a,b}$ satisfying $T_{a,b}(Q_{a,b}) = P_{a,b}$, then $Q_{a,b}$ belongs to L^2 and, denoting by $C_2 = C_2(t)$ the arcs on L^2 joining $Q_{a,b}$ with $P_{a,b}$ then $T_{a,b}(C_2) \subset L^1$.

Finally, denoting by $C_3 = C_3(t)$ the segment on

$$L^3 = L^3(t) = \left\{(x, y) \in \mathbb{R}^2 : x = A - (2b + B)\, y\right\}$$

joining L with $Q_{a,b}$, then $T_{a,b}(C_3) \subset L^2$.

For every $(a(t), b(t)) \in G$, let us denote by R_t the bounded set limited by the arcs C_1, C_2 and C_3. Then, one may check that $T_{a,b}(R_t) \subset R_t$, for every $t \in (0, 2]$. In fact, for $t = 2$, or $(a, b) = (-4, -2)$, one has $T_{-4,-2}(R_2) = R_2$. After this limit situation there always exist critical points inside R_t whose orbits leave the domain R_t, which is no longer invariant. This is also the behaviour of the critical point of the quadratic one-dimensional family $Q_a(x) = 1 - ax^2$ for values of the parameter greater than 2. In [21] a deeper study of the "bidimensional" tent map $T_{-4,-2}$ can be found. In Figure 2, we show the region R_t for $t = 1.8$ and we also remark that, at least for $t \in (0, 2]$, the fixed point, $\widetilde{P}_{a,b}$, given in (6) belongs to the interior of R_t, while the other fixed point, $P_{a,b}$, stays at the boundary of R_t.

Before going into the numerical experiments, we want to end this section by recalling the main conjecture introduced in [21] (see Conjecture 11 there). This conjecture is the natural extension of the results obtained in [14] to the not sectionally dissipative framework in dimension three. In fact, this conjecture motivates some part of the numerical analysis that we are going to show in the next section:

Conjecture 1. *Let $\{f_{a,b}\}_{a,b}$ be a two parameter family of three-dimensional diffeomorphisms and suppose that f_{a_0,b_0} has a dissipative saddle fixed point p_0. Assume that the family $\{f_{a,b}\}_{a,b}$ satisfies the linearization assumption and the eigenvalues λ_1, λ_2 and λ_3 of $Df_{a_0,b_0}(p_0)$ satisfy $|\lambda_1| < 1$ and $|\lambda_3| > |\lambda_2| > 1$. If the invariant manifolds of p_0 have a generalized homoclinic tangency for $(a, b) = (a_0, b_0)$ which*

unfolds generically, then there exists a positive measure set E of parameter values near (a_0, b_0), such that for $(a, b) \in E$ the diffeomorphism $f_{a,b}$ exhibits a strange attractor with two positive Lyapunov exponents.

We think that the right approach to give a positive answer to the above conjecture would be to prove the following one:

Conjecture 2. *For any $0 < c < \log 2$ there exists $t_0 < 2$ and a positive Lebesgue measure set E of values of the parameter t contained in $[t_0, 2]$ such that for any $t \in E$ there exists a dense orbit $\bigcup_{n\in\mathbb{N}} \left\{T_{a,b}^n (x_0, y_0)\right\}$ in R_t, $(a, b) = (a(t), b(t)) \in G$, such that*

$$\left\|DT_{a,b}^n (x_0, y_0)\, \mathbf{v}\right\| \geq \exp(cn),$$

for any unit vector $\mathbf{v}$.

At least, this was the natural route in many other lower-dimensional contexts: To prove the persistence of strange attractors for families of two-dimensional diffeomorphisms (see [2], [14], [19], [20],...) take all the possible information of expansiveness in some related family of one-dimensional transformations (see [1], [8], Chapter 2 in [19],...). By the moment, we give a strong evidence in favour of the conjecture by showing the numerical analysis of the attractors for values of the parameter (a, b) belonging to the curve $G = G(t)$ given in (4), for several values of t in $(1.8, 2)$. For $t \in [0, 1.8]$ the attractor for $T_{a(t),b(t)}$ reduces to the fixed point $\widetilde{P}_{a(t),b(t)}$.

3. **Description of numerical results.** In this section we carry out the numerical experiments showing the attractors arising in the invariant domain R_t of $T_{a,b}$, with $(a, b) \in G$ (see (4)), for different values of $t \in (1.8, 2)$ (recall that, if $t = 2$ then $(a, b) = (-4, -2)$). A few of these experimental results have been already included in a previous paper, see [21]; nevertheless, we also include them here in order to expose a more detailed transformation on the shape of the attractors: We are going to travel from a sink (the global attractor for $t = 1.8$) to an attractor which coincides with the whole invariant domain R_2 (the global attractor for $t = 2$) as it was expected in view of Conjecture 2. Of course, this metamorphosis also arises in the one-dimensional setting for the quadratic family, but the shape of the attractors is very simple in dimension one. In general, the attractors consist of a union of finitely many disjoint intervals (trivial or not). Before going into the details, we want to stress that many of the intermediate attractors appearing between $t = 1.8$ and $t = 2$ would be deserving of a conjecture, similar to Conjecture 2, directed to analytically prove that they are, in fact, one-dimensional or two-dimensional strange attractors and to exactly explain which are the bifurcations leading to the appearance of such attractors. It goes without saying that we believe that the understanding of those transformations far from $t = 2$ would be more complicated: The fact that we have valuable information on the dynamics of $T_{-4,-2}$ (see [21]) would be a very important starting point to investigate what happens for values close to $t = 2$. At least, the same kind of information was essential in many known lower dimensional results.

We will divide this section into several subsections in order to try to present, in order of increasing t, all the mechanisms we have detected (which look essentially different) giving rise to different kinds of attractors.

3.1. **Preparing the family $T_{a,b}$: Description of the numerical methodology.** Let us define the following change of coordinates depending on the parameter

t transforming, for every $t \in G$, the invariant region R_t into R_2:

$$(x, y) \to (\overline{x}, \overline{y}) = \left(\frac{16}{t^4} x + \frac{16\,(2-t)}{t^3} y + 4 - \frac{8}{t}, \frac{8}{t^3} y \right).$$

From the numerical analysis point of view, in spite of the more complicated expression of our family of transformations, this change of coordinates will simplify the monitoring of the evolution of the attractors. In this new coordinates the map $T_{a,b}$ is denoted by $\overline{T}_{a,b}$ and is given by

$$\overline{T}_{a,b}\,(\overline{x}, \overline{y}) = \begin{pmatrix} \frac{1}{4} t^2 \overline{y}^2 + (2-t)\, t\overline{x} + 2\,(t-2)\, t\overline{y} + 12 - 8t \\ \frac{1}{2} t\overline{x} - t\overline{y} + 2\,(2-t) \end{pmatrix}. \tag{7}$$

In the future, we will denote by T_t the respective transformation defined in (7), for which the maximal invariant set is now R_2, independently of the value of t. We also remark that all the numerical experiments showed in this section were designed by taking ten initial conditions uniformly distributed on the critical set of T_t. It is straightforward to check that this critical set still corresponds to those points in R_2 for which $\overline{y} = 0$.

We believe it remains a very interesting new open question related to how the initial points are selected in order to search our attractors:

Remark 1. (Open question) Is it true or not that it is enough to control the orbits of the critical points to capture all the possible attractors?

Of course, we always have in mind the beautiful results prevailing in dimension one, which do not seem to have an easy extension to greater dimensions.

In each one of the pictures displayed along this section, and after dropping an initial transient (generally 10^6 initial iterates), we show between 10000 and 40000 consecutive iterates of each one of the ten orbits mentioned above. We are also able to numerically detect periodic orbits and compute the respective eigenvalues. This would be fruitful to distinguish between the possible local or global bifurcations giving rise to the obtained attractors. Furthermore, the Lyapunov exponents for each one of the obtained attractors can also be numerically approximated up to an error less or equal than 10^{-5}. Hence, as for the numerical viewpoint, in many cases we are able to detect one-dimensional strange attractors (those ones for which the sum and the product of the two Lyapunov exponents are negative) and two-dimensional strange attractors (the sum of the Lyapunov exponents is positive).

Before going on, we present Figure 3.1 where the graphs of the largest Lyapunov exponent and the sum of the two Lyapunov exponents are depicted as functions of the parameter t. The shape of both graphs in different subdomains will be described along the following subsection. Let us sketch how the Lyapunov exponents are numerically obtained: Given a parameter $(a(t), b(t)) \in G$ we take a point (x_0, y_0) which will be assumed to belong to an attractor of $T_{a(t),b(t)}$ (this is obtained by taking an initial transient). Then we take an initial vector, for instance $\mathbf{v_0} = (1, 0)$, define $z_0 = 0$, $\mathbf{w}_0 = \mathbf{v_0}$, and $d_0 = 0$, and iteratively compute, for $n \geq 0$,

$$(x_{n+1}, y_{n+1}) = T_{a,b}(x_n, y_n), \quad \mathbf{w}_{n+1} = DT_{a,b}(x_n, y_n)\mathbf{v}_n, \quad z_{n+1} = \log(\|\mathbf{w}_{n+1}\|) + z_n,$$

$$\mathbf{v}_{n+1} = \frac{\mathbf{w}_{n+1}}{\|\mathbf{w}_{n+1}\|}, \quad d_{n+1} = \log(|\det DT_{a,b}(x_n, y_n)|) + d_n,$$

where we have used the euclidean norm. Observe that, under suitable hypotheses, the real Lyapunov exponents are $\Lambda_1 = \lim_{n\to\infty}(z_n/n)$ and $\Lambda_2 = \lim_{n\to\infty}(d_n/n) -$

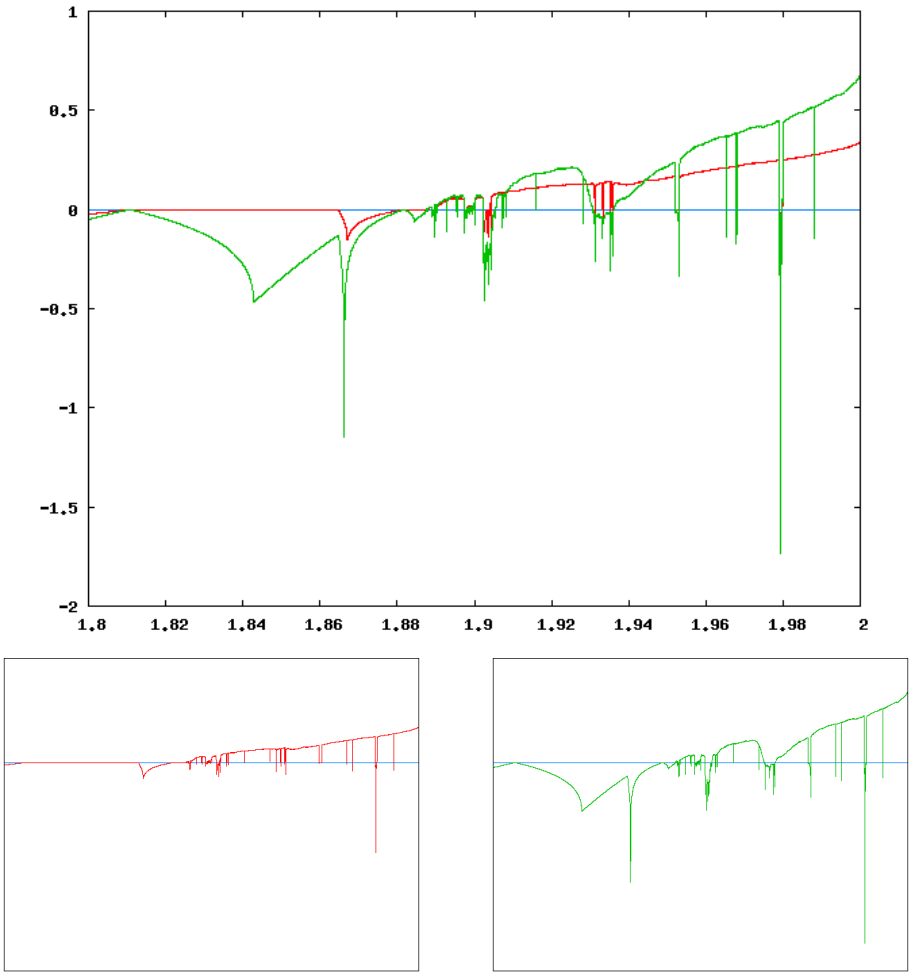

FIGURE 3. Lyapunov exponents as functions of t. On the top picture the graphs of the largest Lyapunov exponent and the sum of the two Lyapunov exponents are shown. We have separately drawn the same two graphs in small pictures below. One thousand equispaced values of t have been taken in all the cases. Moreover, the t axis is drawn in the three pictures.

Λ_1. Then we fix a large number N (in our case we generally have taken $N = 10000$) and compute

$$\epsilon_i = \left| \frac{z_{iN}}{iN} - \frac{z_{(i+1)N}}{(i+1)N} \right| + \left| \frac{d_{iN}}{iN} - \frac{d_{(i+1)N}}{(i+1)N} \right|,$$

for $i = 1, 2, \ldots$ until for certain i, ϵ_i is less than a tolerance ϵ. As we said before, we have taken $\epsilon = 10^{-5}$ for all our computations. Then, we take $\lambda_1 = \frac{z_{iN}}{iN}$ and $\lambda_2 = \frac{d_{Ni}}{Ni} - \lambda_1$ as approximations of the two Lyapunov exponents. If we want to be more confident that the results are precise enough, we ask $\epsilon_i < \epsilon$ for several consecutive values of i. We remark that, in general, we cannot give a rigorous bound of the error in the computation of the Lyapunov exponents. This is related

to the fact that it does not seem possible to compute, unless t is in some exceptional set (for instance $t = 2$), values of parameters for which there exist strange attractors (that is, for which the largest Lyapunov exponent is positive), although it seems that they exist for a large set (in Lebesgue-measure sense) of values of the parameter t.

In a first glance, we see that for many values of t the corresponding map T_t has a two-dimensional strange attractor. The rate of parameters for which this fact happens increases, if we take parameter intervals of the type $[2 - \epsilon, 2]$ for $\epsilon > 0$ small.

3.2. **From sinks to 2D-strange attractors.** We start our analysis by pointing out that, for every $t \in (1.8, 1.8105)$, the attractor for T_t in R_2 reduces to a fixed point which corresponds to the fixed point $\widetilde{P}_{a,b}$ given in (6). This is completely equivalent to what happens for the quadratic unidimensional family $Q_a(x) = 1 - ax^2$ for values of the parameter a smaller than 0.75. Nevertheless, for $t \in (1.8, 1.8105)$, our attracting fixed point is a focus and for some value of the parameter $t^* \approx 1.810535713766$ a Hopf bifurcation occurs, as we have previously computed (see Section 2).

3.2.1. *One-dimensional attractors: Local bifurcations leading to invariant curves.* For the parameter t^* our curve G intersects the Hopf bifurcation line $2b - 4a = 3$, see Figure 2. Therefore, an invariant circle springs. We denote this invariant circle by IC (we follow here the terminology used in [6]). This set IC becomes an attractor for every $t \in (t^*, 1.8649)$. Of course, the fact that the whole invariant curve (a curve densely filled by the orbits) arises also depends on the rotation number of T_t on IC. Let us observe that the largest Lyapunov exponent function vanishes, see Figure 3.2.1, when the rotation number is irrational. This IC attractor cuts the critical line $y = 0$ for some value of the parameter close to $t = 1.84274746\ldots$, where the sum of the two Lyapunov exponents function attains its first minimum value, see Figure 3.2.1. The behaviour of the largest Lyapunov exponent does not contradict the fact that there exists a dense set, with non-empty interior, of values of the parameter t with rational rotation number, because this set has very small Lebesgue measure.

Hence, for this parameter the attractor of T_t contains critical points, just in the same way as the quadratic unidimensional family does for $a = 1$. The set IC for $t = 1.8428$ is the attractor represented in Figure 7a).

As we have introduced in [21], this kind of attractors (invariant circles) were also observed in [6] (among other papers). Let us briefly describe how these attractors appear in [6]: The authors consider the two parameter family of bidimensional noninvertible maps given by

$$L_{a,\tau}(x, y) = \left((1 + a\tau)\, x - \tau xy, (1 - \tau)\, y + \tau x^2\right). \tag{8}$$

This bidimensional family originally appears in a paper of Lorenz, see [11], in which the author studied a sequence of transitions from an attracting fixed point to "computational chaos" (chaotic attractors). These transitions evolved from an attracting fixed point to an attracting invariant circle (IC), and finally to a chaotic attractor. In view of the results obtained in [11], or even similar ones previously obtained in other noninvertible bidimensional cases, see [13], [22] or even [6], it was suggested that this would be a universal "noninvertible route to chaos".

We refer the reader to [6] in which the mechanisms of creation and destruction of invariant circles are described in the invertible and noninvertible frameworks.

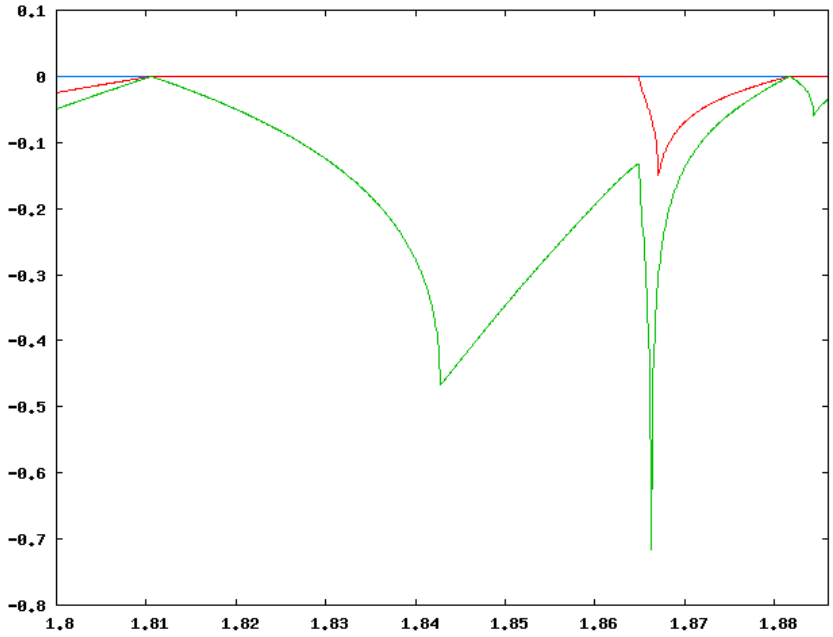

FIGURE 4. Lyapunov exponents as functions of t. Magnification of Figure 3.1 for $t \in [1.8, 1.886]$.

For the invertible case we also cite [3], in which a complete description of those mechanisms is included. As for the noninvertible case, we remark that, in [11], the following scenario for a transition of a smooth IC to a chaotic attractor is proposed as the simplest possible one: As the parameter increases, the IC successively crosses farther over the critical curve, causing it to develop successively sharper features.

Nevertheless, in our setting, we do not detect these sharper features for our attracting IC for values of the parameter t in $(t^*, 1.8649)$. Here, we again point out that our numerical experiments are restricted to the curve $G(t)$ given at (4) and we must say that we do not compute the evolution of our attractor IC outside this line. In any case, if we only select the parameter values in G, our IC is no longer a minimal attractor when the parameter t crosses certain value $t_0 \in (1.8649, 1.86492)$. For this parameter t_0 the curve G enters an Arnold's tongue and an attracting periodic node of period eight appears due to a saddle-node bifurcation. Therefore the largest Lyapunov exponent becomes negative, see Figure 3.2.1. This attracting periodic orbit survives in the range of parameters $(t_0, 1.88165)$, but for some value in the above interval their eigenvalues become complex. In any case, beyond $t = t_0$, we do not see in G the set IC showed in Figure 7a) anymore. Moreover, the IC becomes only continuous (see [3]) until the attracting periodic orbit undergoes a Hopf bifurcation, when a 8-pieces attracting invariant curve appears.

However, the presence of invariant circles developing sharper features, as was described in [6] and [11], becomes also patent in our situation for greater values of the parameter t (henceforth, for parameters (a, b) in G): In Figure 7e) it is shown the shape of one piece of an 8-pieces attractor that emerges from the eight periodic orbit arising at $t = t_0$. Namely, the periodic orbit undergoes the above mentioned

Hopf bifurcation for some value of the parameter t in $(1.88165, 1.88166)$ giving rise to an attractor formed by eight invariant circles, that we denote by IC8. Figure 7b) shows IC8 for $t = 1.88624$ (see also Figure 7c), in which an amplification of one of these eight pieces is shown).

3.2.2. *Destruction of invariant curves: Global bifurcations leading to 1D strange attractors.* In order to follow the transition from Figure 7c) ($t = 1.88624$) to Figure 7e) ($t = 1.88762$) we refer the reader once again to [6] where the authors definitively associate the destruction of IC´s for the family given in (8) to the presence of global bifurcations, i.e., homoclinic or heteroclinic bifurcations (created from the intersections of invariant manifolds of periodic orbits which stay very close to the IC) which precede to the reappearance of an attractor, this time chaotic with loops (see Figure 7e), where the piece of the attractor is no more homeomorphic to a circle). In fact, as we can read at [5], loops and cusps are usually observed on invariant curves for noninvertible maps. Of course, the existence of homoclinic bifurcations leads to the presence of high–periodic attractors and probably (one-dimensional) strange attractors, see [14]. This would explain the shape of the attractor represented in Figure 7d) for the value of the parameter $t = 1.88758$. For this special value of the parameter we numerically obtain a positive Lyapunov exponent: In fact this numerical value corresponds to 2.09×10^{-4} (recall that we numerically approximate Lyapunov exponents up to an error less than 10^{-5}). Therefore we find our first value of the parameter for which there exists a strange attractor, which as it was expected corresponds to a one-dimensional strange attractor. Moreover, the same can be said about the attractor displayed in Figure 7e) ($t = 1.88762$) since the numerically obtained Lyapunov exponents are 8×10^{-4} and -6.94×10^{-3}. In Figure 3.2.2 we show the evolution of the largest Lyapunov exponent and the sum of the two Lyapunov exponents for $t \in (1.886, 1.8877)$.

3.2.3. *Two-dimensional strange attractors.* Once the IC8 disappears the attractor becomes chaotic, see Figure 7f) in which the continuation of the piece of the 8-pieces previous attractor is shown. The sum of the Lyapunov exponents for this value of the parameter ($t = 1.88773$) is positive. In fact, the numerically obtained exponents are 1.49×10^{-3} and -8.4×10^{-4}. Therefore, for this value of the parameter we obtain our first two-dimensional strange attractor. See Figure 3.2.3 where the Lyapunov exponents functions are depicted for $t \in (1.8877, 1.889)$.

Therefore, at sight of the six pictures appearing in Figure 7 it seems clear that the transition from periodic attractors to chaotic attractors is a phenomenon which must occur not only for the bidimensional families studied in [6] and [11], but also in simpler situations (observe that the expression of our family (3) is substantially less complicated than the one given in (8)) and, even more important, in more generic frameworks: Three-dimensional diffeomorphisms unfolding homoclinic tangencies associated to fixed points whose unstable manifold has dimension two.

3.3. **Coexistence of attractors.** Furthermore, by increasing the value of t we also obtain more interesting situations which we are going to describe. In Figure 8, one may observe how two different attractors coexist for $t = 1.889$. One of them (the one displaying a bidimensional structure) is the continuation of the attractor described in Figure 7f) and therefore is one of the pieces of an 8-pieces bidimensional attractor. A numerical analysis gives two positive Lyapunov exponents for this 2D attractor (this is our first value of t for which this fact happens). From the topological point of view it is interesting to note that, for $t = 1.889$, the inner hole exhibited by

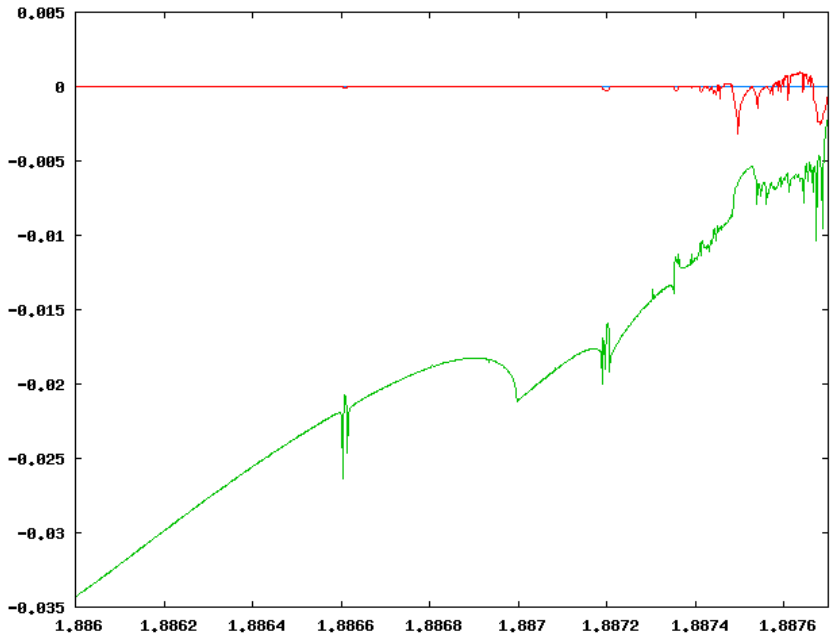

FIGURE 5. Lyapunov exponents as functions of t. Magnification of Figure 3.1 for $t \in [1.886, 1.8877]$.

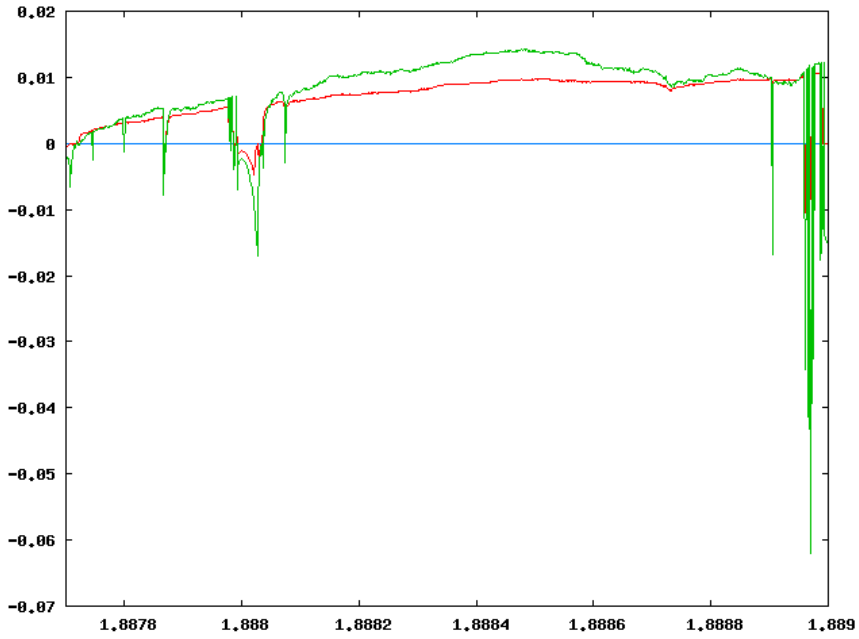

FIGURE 6. Lyapunov exponents as functions of t. Magnification of Figure 3.1 for $t \in [1.8877, 1.889]$.

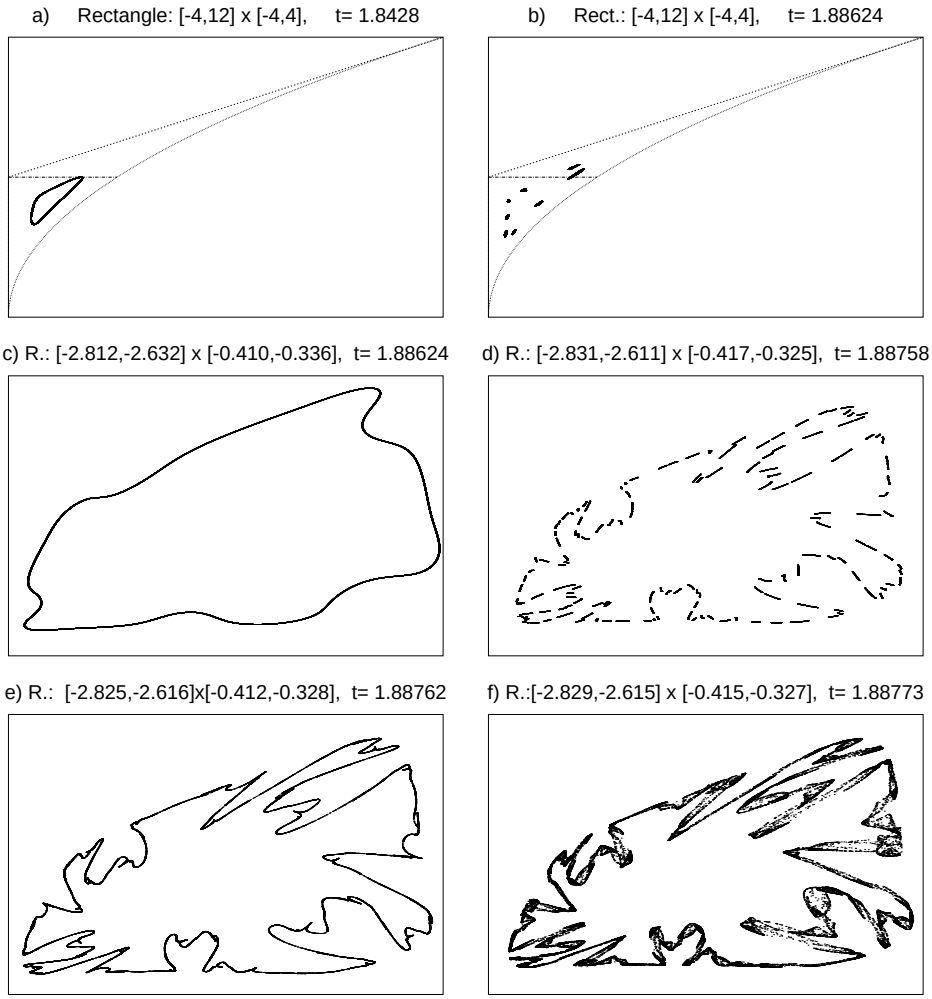

FIGURE 7. Attracting sets for different values of t. In Figures a) and b) we have also drawn the region R_2 and the critical line. In Figures c), d), e) and f) we have drawn the evolution of the same component of the eight-pieces attractor.

the attractor in Figure 7f) disappears (this phenomenon is frequently observed for our family T_t in several subdomains of the range of parameters $(1.8, 2)$, and it will be described in a more detailed way in subsection 3.4). This also happens in the quadratic family for values of the parameter slightly bigger than 1, for which the attractor lives in two disjoint intervals leaving the fixed point (which is a repellor) between them. Moreover, the boundary of those intervals are positive iterates of the critical point. As increasing the parameter for the quadratic unidimensional family $Q_a(x) = 1 - ax^2$ these disjoint intervals containing the attractor collapse when the third iterate of the critical point coincides with the fixed repelling point: See also Section 5 where more similarities with the quadratic family are exposed.

Of course, it is not hard to prove the existence of a 8-periodic repellor inside the hole of the attractor for Figure 7f) which plays the role of the fixed point for the quadratic family and takes part of the 2D attractor in Figure 8. Therefore, it is natural to expect that the inner hole of the 2D attractor disappears when some critical point belongs to the closure of the unstable set of this 8-periodic repellor.

In Figure 8, a new one-dimensional attractor can be seen. One piece (homeomorphic to a circle) of a 27-pieces attractor is shown (Figure 8c), compare also with subsection 3.2.1). This attractor will be destroyed for some slightly bigger value of the parameter due to a new Hopf bifurcation. After this value of the parameter three different attractors coexist for $t = 1.88949$, see Figure 9a). The continuation of the 2D attractor described above, the 27-periodic attractor coming from the Hopf bifurcation and a new one-dimensional attractor formed by 54 pieces, coming from a period doubling cascade of bifurcations. In Figure 9b) two points of the attracting periodic orbit are represented by crosses, and two pieces of the 54-pieces 1D strange attractor can be seen. This new 1D attractor rises in a similar way as for the Hénon map: The map T_t undergoes a dissipative saddle-node bifurcation of period 54 at $t \approx 1.889409$. After a period doubling cascade of bifurcations it becomes a 1D strange attractor of Hénon type (one of the Lyapunov exponents along the 1D attractor of Figure 9c) is 6.06×10^{-3}). Here, we also refer the reader to Figure 21 where the rate of initial conditions travelling to different attractors is displayed for values of t in the interval $(1.888, 1.899)$.

On the other hand, the numerically obtained Lyapunov exponents for the 2D attractor in Figure 9 ($t = 1.88949$) are both positive and, in order to show the reliability of our numerical method for computing Lyapunov exponents we remark that the obtained exponents along the attracting periodic orbit are -1.77495×10^{-2} and -1.77496×10^{-2} (we point out that the respective periodic orbit is a focus and, therefore, the "real" Lyapunov exponents coincide).

Figure 9c) is devoted to show the geometry (overall, it is remarkable the presence of self-intersections) of one of the pieces of the unidimensional attractor introduced in Figure 9a), while in Figures 10a), b) and c) we successively enlarge some region of the 2D attractor (the obtained exponents are 1.142×10^{-2} and 3.78×10^{-3}) in order to confirm the presence of a periodic repellor (which is a 40-periodic focus whose eigenvalues have modulus very close to 1) and also of a 120-periodic saddle. The shape of part of the unstable set of this periodic saddle corresponds to the more marked curves ("more visited regions") in Figure 10c). In Figure 10d) we have drawn the invariant manifolds of the 120-periodic saddle in the same rectangle of Figure 10c). We see inside the region determined by the unstable invariant manifold, the 40-periodic repeller focus. It is interesting to notice that this focus is near a 1:3 resonance. A study of this bifurcation, including the bifurcation diagram of the approximating flow can be found in [10].

3.4. **Joining strange attractors: Heteroclinic bifurcations.** As the parameter increases, the size of the 8-pieces 2D attractor of the previous figures grows due to the existence of inner "tongues" (one of them marked with an arrow), which will connect, for bigger values of the parameter, the eight pieces of the attractor to give rise to the first 1-piece 2D attractor. In Figure 11a) we can see the tongues of one piece of the 8-pieces 2D attractor for $t = 1.8912$ (one of them is marked with an arrow), jointly with two saddle points p and q with their invariant manifolds. Both points p and q belong to a 16-periodic orbit. Moreover, in Figure 11b) we have represented in a larger rectangle, three pieces of the 8-pieces 2D attractor, six

points of a 16-periodic saddle and the unstable invariant manifold of one of these points, which we call p in the picture.

In Figure 12 there is a 1-piece 2D attractor with a hole, for $t = 1.892$. The union of the 8-pieces 2D strange attractor into 1-piece is due to the birth of a heteroclinic intersection between the 8-periodic repellor inside the 8-pieces attractor and a 16-periodic expansive saddle near the 2D attractor, whose unstable invariant manifold connects the pieces of the attractor, as we can deduce from the previous figures. By a stronger density of points, one may still detect the shape of the previous 8-pieces attractor plotted in Figure 11a). We also may distinguish how its inner "tongues", which have been described above, are larger than those in Figure 11a).

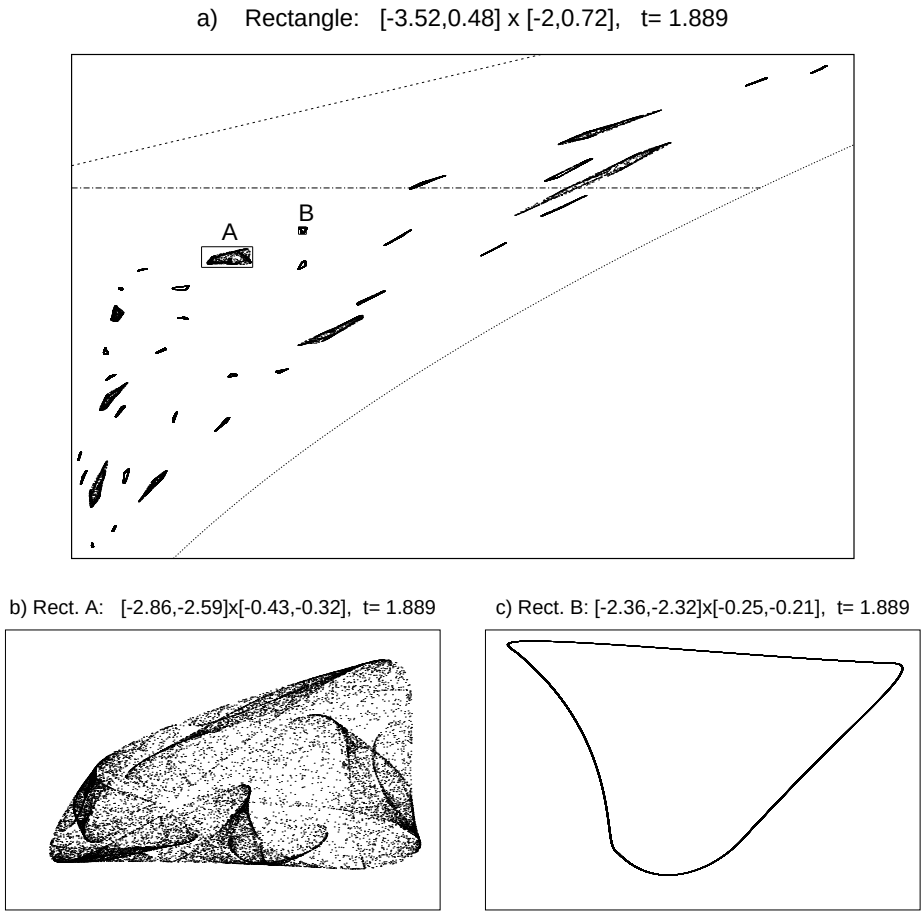

FIGURE 8. Attracting sets for $t = 1.889$. Figures b) and c) are, respectively, magnifications of one piece of the two-dimensional attractor and the IC.

The attractor given in Figure 12 is a 2D strange attractor whose numerically obtained Lyapunov exponents are both positive: 3.655×10^{-2} and 8.341×10^{-3}. Of course, in the inner hole of the attractor there exists a fixed repellor (in fact, the respective fixed point $\widetilde{P}_{a,b}$ given in (6)). Therefore, the evolution of this attractor is

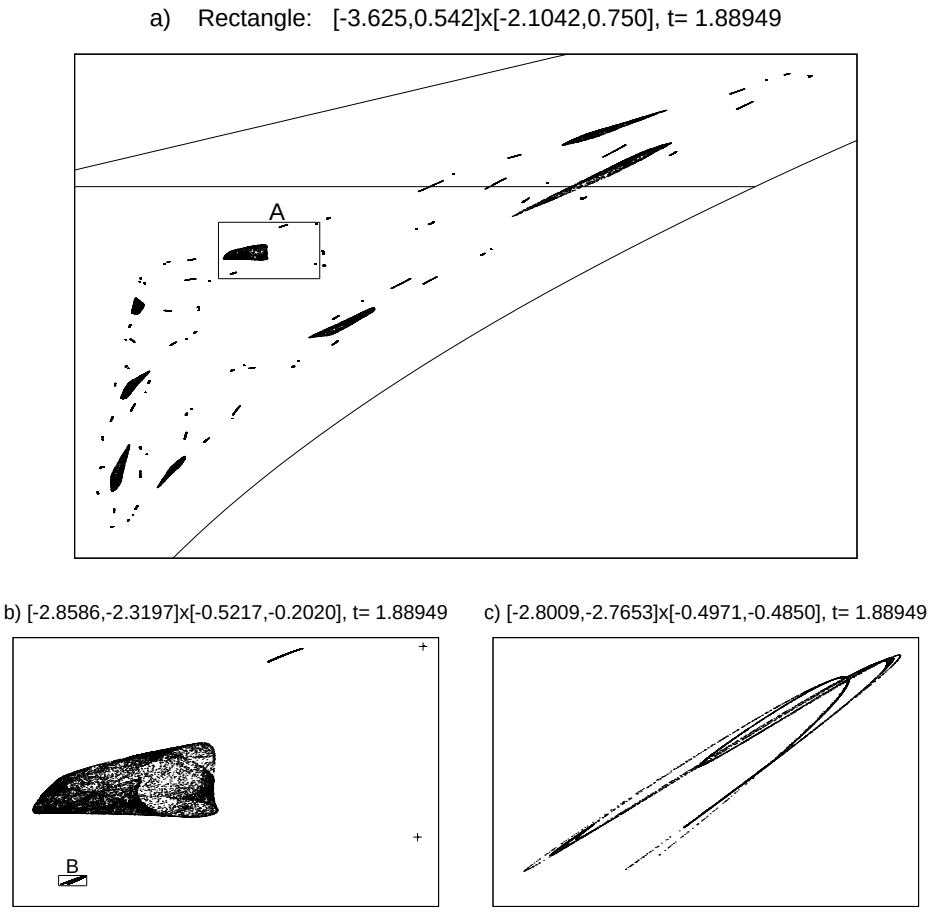

FIGURE 9. Attracting sets for $t = 1.88949$. Figure b) is a magnification of the rectangle A. The two crosses appearing in this window represent two iterates of a 27-periodic attractor. Figure c) is a magnification of the rectangle B.

very similar to the one described from Figure 7f) to Figure 8b): A 2D attractor with an inner hole, the size of the hole decreasing as long as the parameter increases (see subsection 3.3). This hole definitively disappears when some critical point belongs to the closure of the unstable set of $\widetilde{P}_{a,b}$. Nevertheless, now the whole process follows in a large set of parameters; namely, the 1-piece 2D attractor without hole does not arise until $t = 1.9302$. Moreover, in the interval of parameters $(1.892, 1.9302)$ there are other interesting situations which we must describe. See Figure 13 where the Lyapunov exponent functions (the largest exponent and the sum) are displayed for this range of parameters.

3.5. **Travelling to $t = 2$.** The 2D strange attractor appearing in Figure 12 vanishes due to local bifurcations: Some periodic point becomes an attractor for some parameter in $(1.89276, 1.89278)$. Furthermore, along the range of parameters $(1.89278, 1.89992)$ many already described bifurcations take place: There exists an

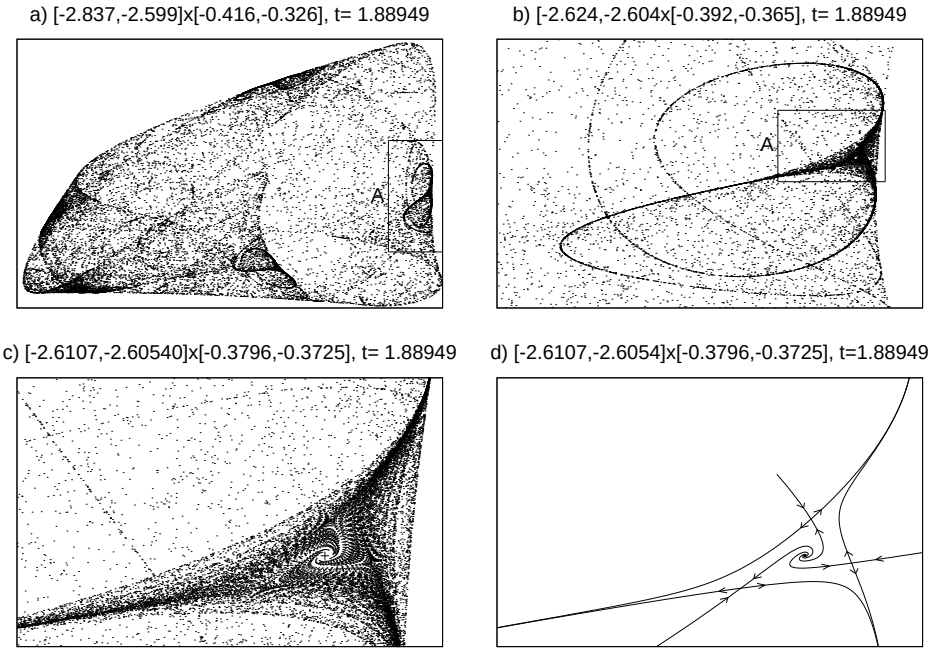

FIGURE 10. Left up: Magnification of the 2D attracting set of Figure 9b). Right up: Magnification of the rectangle A of the previous figure. Down left: Magnification of the rectangle A of the previous figure. Down right: The same rectangle of the previous figure, with the invariant manifolds of the 120-periodic saddle.

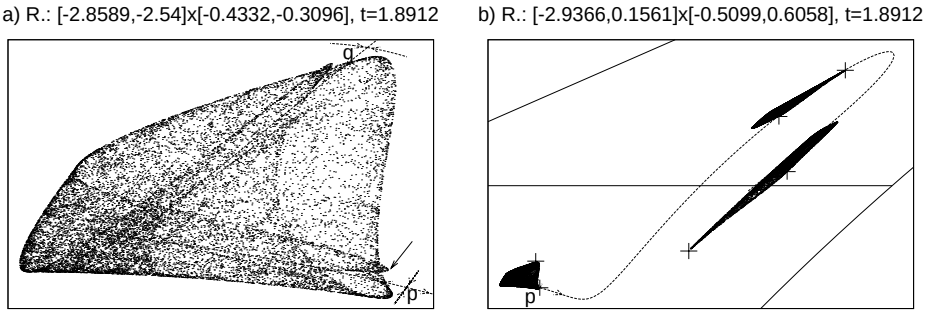

FIGURE 11. a) A piece of a 8-pieces 2D attractor with "tongues" and two iterates of a 16-periodic saddle jointly with their invariant manifolds. b) Three of the pieces of the 8-pieces attractor, jointly with 6 iterates of a 16-periodic saddle, represented by crosses. Moreover, the unstable invariant manifold of the point p is included.

11-periodic attracting orbit which is transformed through a Hopf bifurcation into a 11-circles attractor (see subsection 3.2.1). This attractor follows the bifurcation scheme announced in [6]: The one-dimensional attractor formed by circles which are

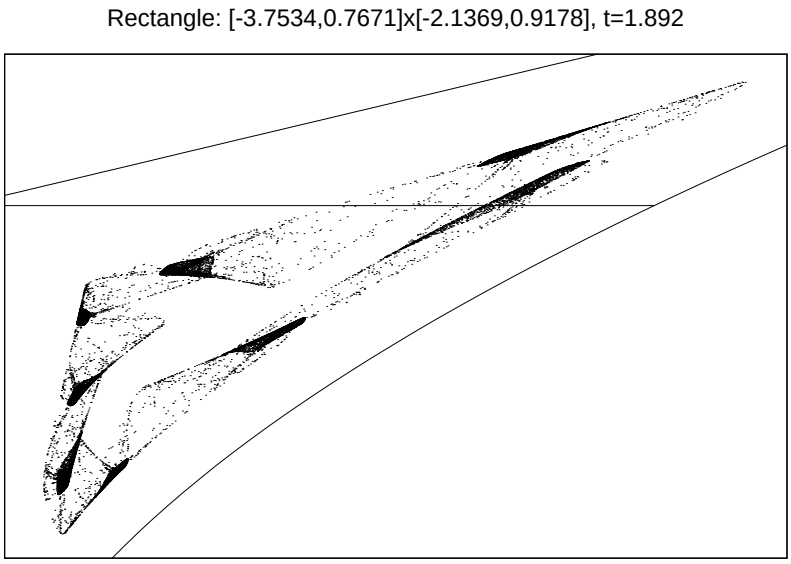

FIGURE 12. A 1-piece 2D strange attractor.

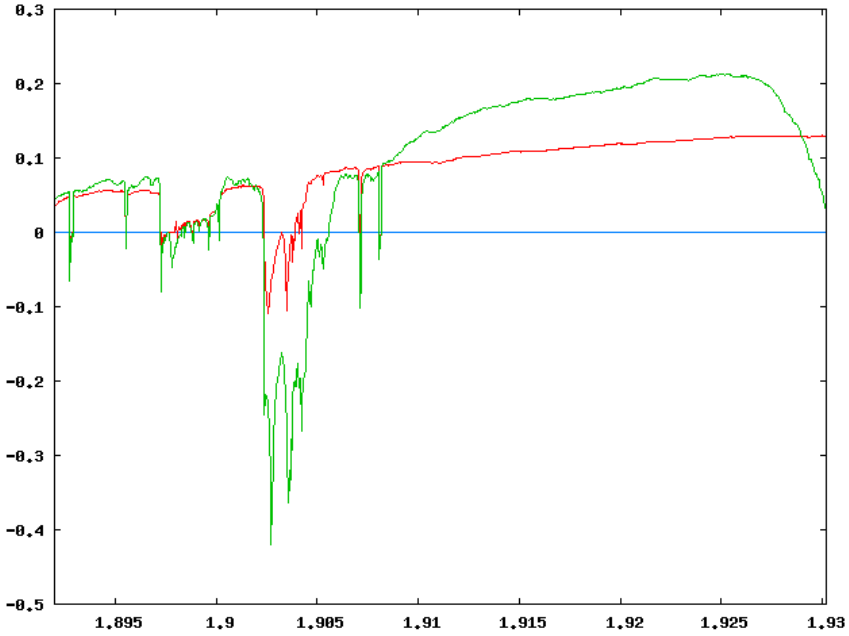

FIGURE 13. Lyapunov exponents as functions of t. Magnification of Figure 3.1 for $t \in [1.892, 1.9302]$.

close enough to periodic saddles whose invariant sets collapse and these homoclinic or heteroclinic bifurcations involve the appearance of chaotic attractors, see subsections 3.2.2 and 3.2.3. At the same time, the same holds for a 22-pieces attractor which, for some open set of parameters coexists with the above one. However, this new attractor experiments the same sequence of bifurcations described along Section 3.2, but in inverted sense: As the parameter increases this 22-pieces attractor evolves from a chaotic attractor to a periodic one. Let us illustrate these parallel processes followed by these two attractors with several numerical experiments.

In Figure 14a) we may see the global layout in R_2 of these two attractors for $t = 1.898$. By making a magnification near the critical line, see Figure 14b), we distinguish one piece of the 11-pieces attractor, which is homeomorphic to a circle (IC11), and two pieces of the 1D strange attractor. On this last attractor the obtained exponents are 1.3443×10^{-3} and -2.8673×10^{-2}. A numerical analysis also allows us to detect, very close to both attractors, a 22-periodic expanding saddle (the product of its eigenvalues is bigger than one) which is the candidate to produce chaotic attractors from IC11, see explanations in subsection 3.2.2. In Figure 14c), two points of this 22-periodic orbit are represented by crosses.

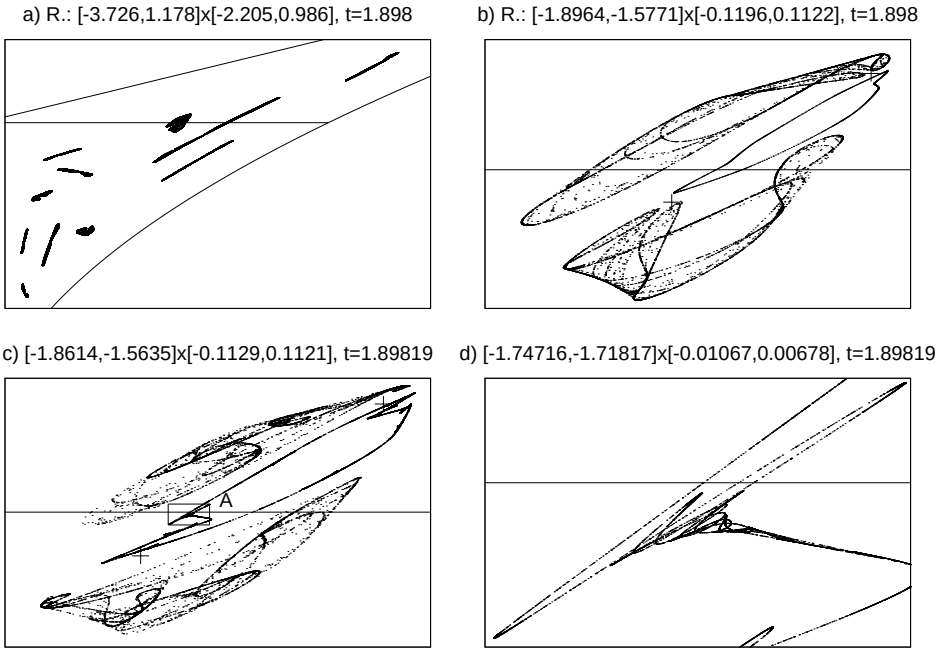

FIGURE 14. Several attractors inside the region R_2. The critical line and the boundary of R_2 are included and the crosses are periodic points of period 22. Figure b) is a magnification of a), and d) is a magnification of rectangle A in Figure c).

As was expected, for slightly large values of the parameter the IC11 is no longer homeomorphic to circles, see Figure 14c) in which both attractors are represented for $t = 1.89819$. The 11-pieces attractor exhibits loops (cusps have not been observed) according to the magnification made in Figure 14d). This situation is, once again,

the prelude to the birth of chaotic 2D attractors instead of 1D attractors, as was described in subsections 3.2.2 and 3.2.3. For this value of the parameter the 11-pieces attractor already presents a positive Lyapunov exponent.

After homoclinic or heteroclinic bifurcations, the continuations of these two attractors are shown in Figure 15a) for $t = 1.898244$. The previous 1D attractor breaks into several pieces, one of them represented in the next picture, see Figure 15b). In fact, it seems to be a unidimensional set with self-intersections which probably arises in the vicinity of homoclinic orbits associated to a 198-periodic saddle, represented in this figure by a cross. For both attractors in Figure 15a), one of the Lyapunov exponents is positive and the other one is negative.

In order to follow the competition between these two different attractors (see also subsection 3.8) one may repeat the numerical experiments from Figure 14a) to Figure 15a), by taking twenty initial conditions uniformly distributed on the critical line. It is remarkable that, in Figure 14a) the 11-pieces attractor only captures three of these twenty orbits (the remainder travel to the 22-pieces attractor) while for the situation given in Figure 15a) thirteen initial conditions go the 22-pieces attractor and seven do to the other one. See again Figure 21 where the rate of initial conditions travelling to different attractors for values of $t \in (1.888, 1.899)$ is shown.

In fact, for $t = 1.89827$ (see Figure 15c)) the 22-pieces attractor decomposes into 12×22 unidimensional pieces. After new homoclinic or heteroclinic bifurcations this 22-pieces attractor turns homeomorphic to circles, according to Figure 15d) ($t = 1.898884$) just in the same way as it was described in subsection 3.2. Inside these circles one can find a 22-periodic repelling focus near a Hopf bifurcation. The size of the 11-pieces attractor grows and, in fact, the sum of its Lyapunov exponents becomes positive. We note that a previous 198-periodic saddle ($t = 1.89819$) inside this attractor becomes a repellor and a 99-periodic expansive saddle is born by a saddle-node bifurcation. We have included in the corresponding figure, part of the continuation of this 99-periodic expanding saddle. It can be seen that all these saddle points have heteroclinic intersections with the neighbour one. Hence, the transition of this attractor was given in subsection 3.4.

For $t = 1.89919$, see Figure 15e), there only exists one attractor, which is the continuation of the previous 11-pieces 2D strange attractor, but now with 5×11 2D pieces. The other one disappears once a new Hopf bifurcation and a new saddle-node bifurcation take place. It is interesting to note that in this case, inside all the pieces, there is a 55-periodic slightly dissipative saddle. It seems that the closure of its unstable invariant manifold is a 2D set, because the sum of the Lyapunov exponents of the attractor are positive but small.

For $t = 1.8992$, see Figure 15f), there only exists one attractor: The continuation of the 5×11-pieces 2D strange attractor described before, which is now again a 11-pieces attractor due to the appearence of homoclinic and heteroclinic bifurcations (see subsection 3.4). We again observe the existence of "tongues" inside the 2D attractor. These "tongues" will be, once again, the cause of the appearance of a global 1-piece 2D attractor, see Figure 3.5a) for $t = 1.9$, like the one studied in subsection 3.4 (see also Figure 12). The shape of the attractors giving rise to the 1-piece 2D one is quite similar in both cases: Bidimensional pieces with "leaving tongues". The only difference in the last case is that we have not found a heteroclinic bifurcation with an expanding saddle when the attractor becomes int a one piece attractor.

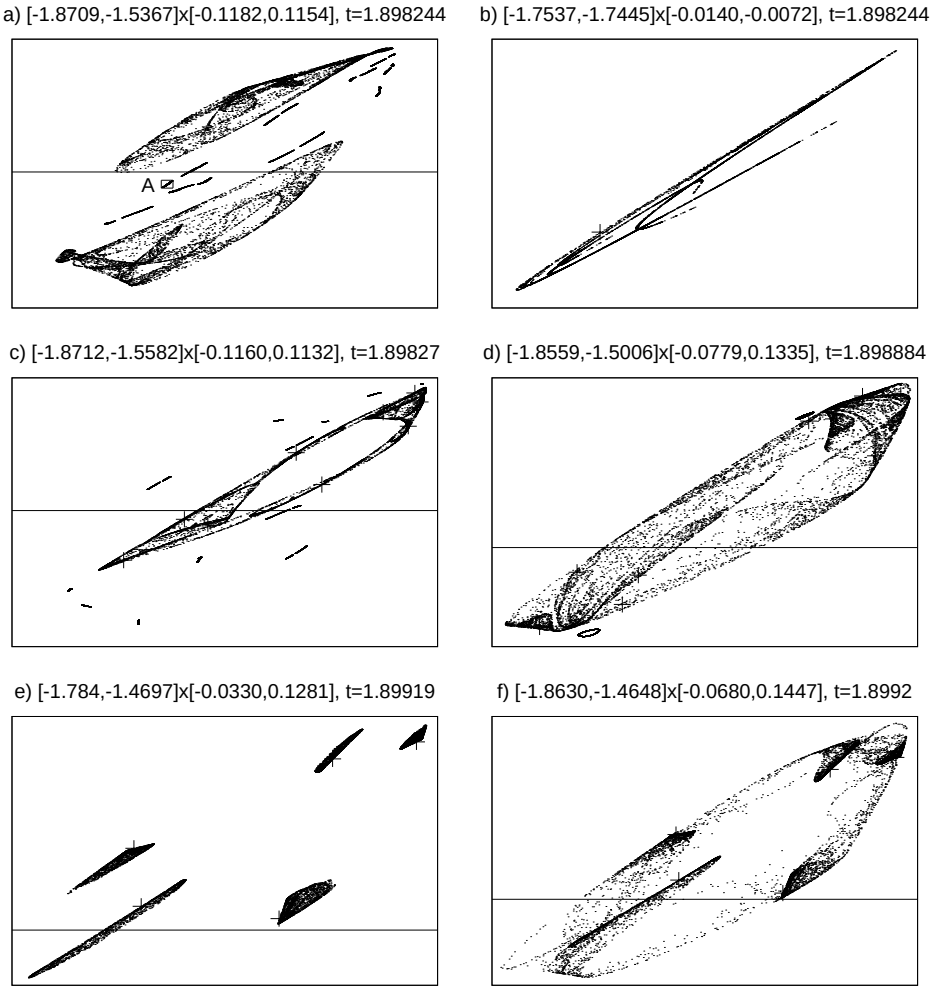

FIGURE 15. a) Evolution of the attractors of Figure 14. Figure b) is a magnification of the rectangle A of a). The cross indicates the existence of a 198-periodic saddle. In Figure c) part of a 99-periodic expansive saddle is marked with crosses. In Figure d), the crosses are again part of a 99-periodic expanding saddle. In Figures e) and f) the crosses are 55-periodic saddles.

The size of the attractor showed in 3.5a) is bigger than the size of the one obtained in Figure 12. This common phenomenon for passing from 2D attractors with inner holes to 2D attractors without holes can be observed several times along the numerical analysis for 2D attractors, see subsection 3.4. In any way, before the 2D 1-piece global attractor without holes arises, new local bifurcations of periodic points for some value of the parameter in $(1.90012, 1.900123)$ bring about the appearance of a 44-pieces attractor. See Figure 3.5b) to check the global arrangement of this attractor for $t = 1.900123$, and also Figure 3.5c) in which one of its pieces is represented. In this case one of the Lyapunov exponents is positive although the

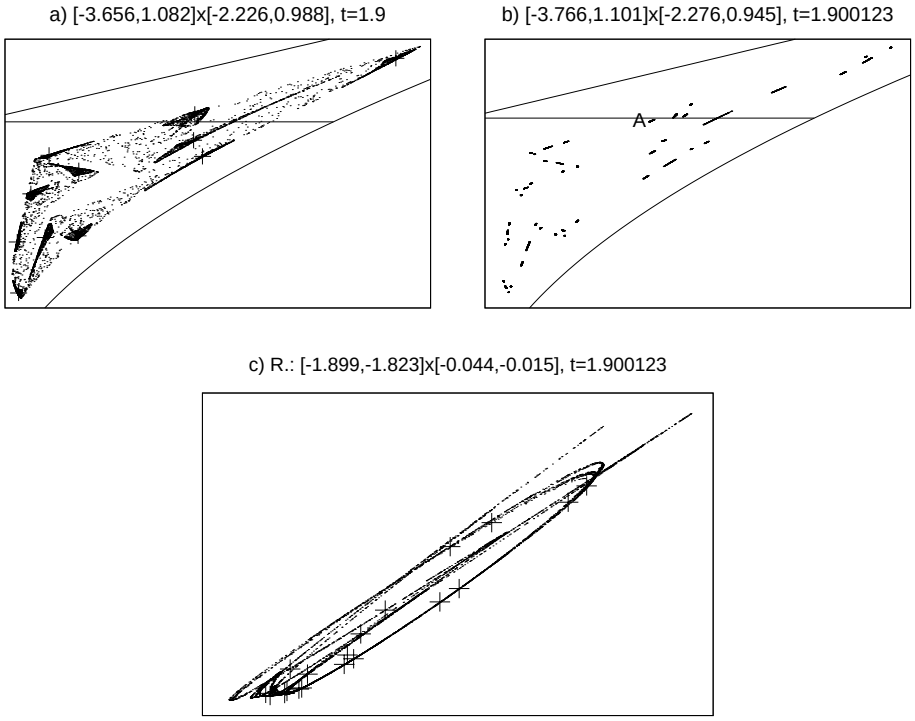

FIGURE 16. a) 1-piece 2D strange attractor. The crosses indicate points of a repelling focus of period 11. b) Evolution of the previous attractor. c) Magnification of the piece A of the 44-periodic attractor of the previous figure. The crosses indicate periodic points. See the explanation in the text.

sum of both exponents is negative. See also Figure 13 to follow the evolution of our two Lyapunov functions. Moreover in Figure 3.5c) we have drawn 9 points of each one of two periodic saddle orbits of period 396 ($= 9 \times 44$) that seem to be inside the attractor, and one 44-periodic repelling focus in the hole inside the attractor. One of the saddles is expansive and the other one is dissipative, but the sum of the Lyapunov exponents of the attractor is slightly negative.

Let us point out that by taking 10^4 equidistant parameters in the set $(1.9, 2)$, most of the obtained situations have been already observed for certain windows in the domain of parameters $(1.8, 1.9)$.

3.6. **New kinds of attractors.** In this subsection we will introduce not only those numerical experiments which seem to offer new kinds of attractors, but also those ones which may clarify some of the previously explained bifurcations.

3.6.1. *Triangular attractors.* For $t = 1.901208194$ we have a 36–pieces 2D strange attractor with a hole inside every piece. In Figure 17a) we have drawn one of the pieces of this attractor. We note that surrounding the hole in this attractor, there exists a triangular region where there is more density of points of the attractor. Near each vertex of this triangle one iterate of a 108 (3×36) expanding periodic

saddle is located, whose unstable invariant manifold is contained in the attractor. We have also drawn a point inside the hole that belongs to a repelling focus orbit of period 36. Changing slightly the parameter ($t = 1.901208196$) we see that the 36-pieces attractor now is a thick triangle, and the rest has disappeared (see Figure 17b)). This is because for some intermediate t the map has undergone a heteroclinic tangency between the unstable invariant manifold of some saddle in the thick triangle and the stable invariant manifold of the 108-periodic saddle near the vertices of the triangle. For $t = 1.90120842$, a 108-pieces 2D strange attractor and a 36-pieces attracting invariant curve with triangular shape, coexist (see Figure 17c)). The 2D attractor is destroyed when a heteroclinic intersection between the stable invariant manifold of the 108-periodic saddle near the vertices of the triangular invariant curve, and the unstable invariant manifold of some 108-periodic repellor inside the 2D attractor, takes place for a slightly small value of t. In Figure 17d) there is a magnification of Figure c), where the invariant manifolds of one of the saddle points are drawn.

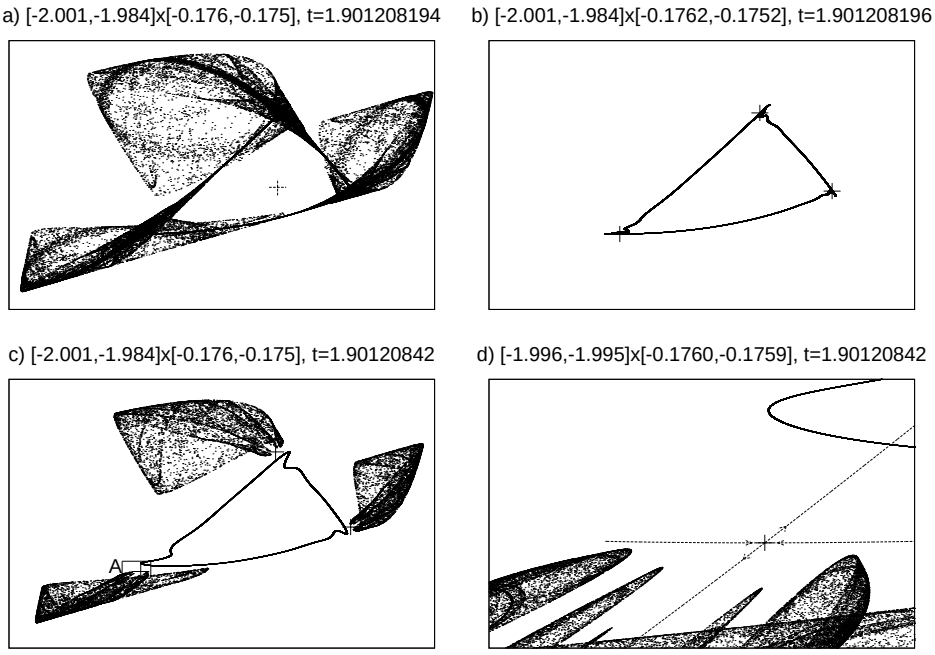

FIGURE 17. a) One piece of a 36-pieces 2D strange attractor. The cross indicates a point of a repelling focus of period 36. b) One piece of a 36-pieces 1D strange attractor. The crosses indicate points of a 108-periodic saddle. c) Three pieces of a 108-pieces 2D strange attractor, one piece of a 36-pieces attracting invariant curve, and three points of a 108-periodic saddle. d) Magnification of the rectangle A of the previous figure. The invariant manifolds of the saddle are drawn.

3.6.2. *An expanding saddle unstable set attractor.* In Figure 18a) we present a new class of attractor for $t = 1.9379$. Since the obtained exponents are 0.12982 and

-0.078 we are dealing with an expanding map. In spite of several windows of sinks, this attractor is born from the already mentioned global 1-piece 2D attractor without holes. The respective bifurcation probably takes place due to heteroclinic bifurcations between the invariant manifolds of periodic points. In fact, one may numerically detect a 3-periodic expanding saddle inside the attractor and also a 3-periodic repelling node. The attractor must correspond to the closure of the unstable set of the 3-periodic expanding saddle and must be contained in the unstable invariant set of the repelling node. In Figure 18b) we have drawn a magnification of one of the pieces of this 2D strange attractor.

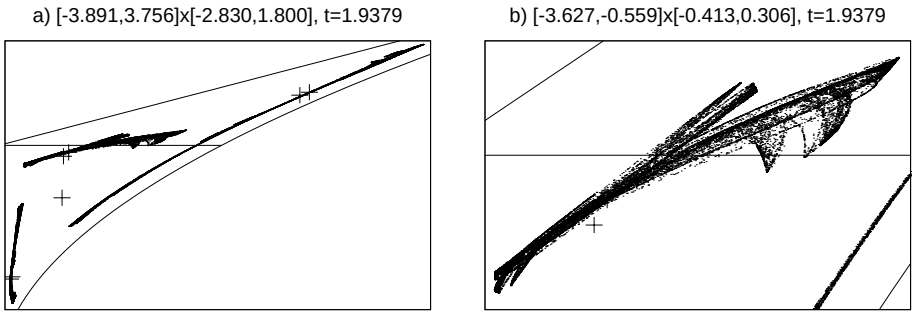

FIGURE 18. a) A 3-pieces 2D strange attractor. The crosses inside the attractor represent a period three expanding saddle, and near this periodic saddle, it is also represented a 3-periodic expanding node near, but outside the attractor. The cross on the central part of the picture is a repelling 1-periodic focus. b) Magnification of one of the pieces of the attractor.

The fact that the attractor in Figure 18 coincides with the closure of the unstable manifold of an expanding periodic orbit with real eigenvalues probably explains the fact that its geometry is substantially different from the one exhibited by the previously obtained several-pieces 2D attractors: These last ones always seem to correspond to the unstable set of repelling periodic foci. In any case, the future evolution of the attractor in Figure 18 was already observed (see subsection 3.4): As the parameter increases the size of its pieces grows until a new global heteroclinic bifurcation takes place: Interaction with the stable set of the 1-periodic repelling focus (see the cross in the central part of Figure 18a) outside the attractor) produces the new appearance of the 1-piece 2D global attractor without holes for a certain value in the range of parameters $(1.944, 1.95)$.

3.6.3. *Joining Hénon-like attractors.* The first five pictures in Figure 19 are devoted to explore a new global bifurcation. The process starts in Figures 19a) and b) where a 32-pieces 1D strange attractor emerges for $t = 1.97981$. In Figure 19b) eight of these pieces are displayed (inside each piece we have represented with a cross an iterate of a 32-periodic dissipative saddle). Each one of them seems to be a Hénon-like strange attractor associated to the displayed dissipative saddle, which probably shows up from a heteroclinic or homoclinic bifurcation. In fact, several expanding and dissipative saddle periodic points are found in the set of parameters $(1.97981, 1.97987)$ close to the respective attractor.

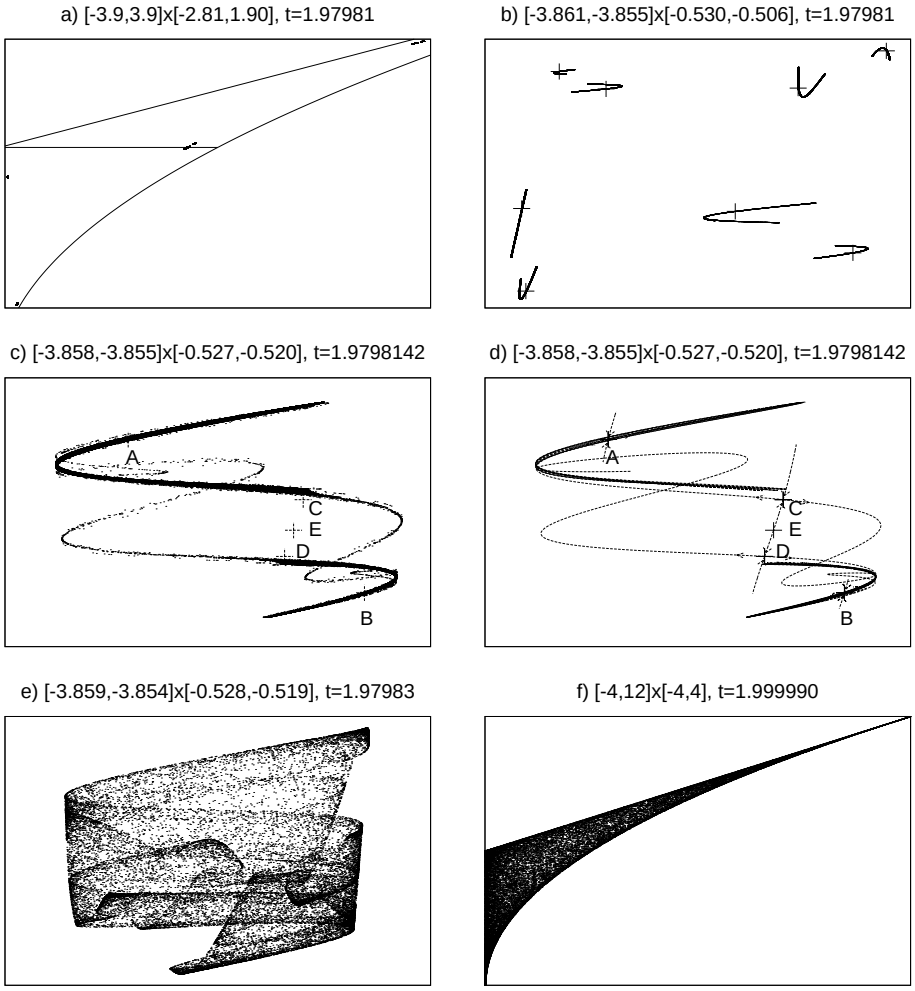

FIGURE 19. a) A 16-pieces 1D strange attractor. b) Magnification of eight pieces of the previous figure. c) One piece of a 16-pieces 1D strange attractor. The points A and B belong to the orbit of a 32-periodic dissipative saddle, C and D to a 32-periodic expanding saddle orbit and E to a 16-periodic repelling node orbit. d) The same parameter t and the same rectangle of the previous figure with the invariant manifolds of the previous periodic points. e) Evolution of the same piece of the previous attractor for $t = 1.97983$. f) The whole attractor for $t = 1.99999$.

The pieces of the attractor in Figure 19b) collapse two by two to form a 16-pieces 1D strange attractor for $t \approx 1.979814$. In Figure 19c) one piece of this new attractor can be seen.The Lyapunov exponents for this value of the parameter are 0.02027 and -0.0261. We have drawn also two points of a 32-periodic weakly expansive saddle, whose unstable invariant manifold generated the previous 32-pieces 1D strange attractor (also see subsection 3.6.2), two points of a 32-periodic

expanding saddle and one point of a 16-periodic repelling node outside the attractor. Nevertheless, the presence of repelling nodes, expanding saddles and the possible interactions between their invariant manifolds would be very relevant in order not only to justify the complicated geometry of these attractors but also to understand what kinds of bifurcations lead to them. In Figure 19d) we have represented the invariant manifolds of the 32-periodic points of the previous figure. We notice that $W^u(C)$ and $W^u(D)$ have intersections respectively with $W^s(A)$ and $W^s(B)$. Moreover, $W^u(A)$ and $W^s(C)$ have an intersection that is near to be tangent. This is also the case of $W^u(B)$ and $W^s(D)$. All these heteroclinic intersections explain why the 32-pieces attractor has become a 16-pieces attractor. Finally, we notice that points C and D have been born by a flip bifurcation of the point E.

In Figure 19e) we may see the continuation of one piece of the above 16-pieces attractor for $t = 1.97983$. The sum of the Lyapunov exponents is now positive. Moreover, the hole inside the attractor has disappeared. This is because one of the saddles has become a repelling node, and the unstable invariant manifold of this node has intersections with the stable invariant manifold of the 16-periodic repelling node. If $t = 1.97987$ the whole attractor has four pieces (once again, several pieces of the old attractor collapse probably due to heteroclinic bifurcations) with a hole, where there is a 4-periodic repelling focus, similar to other previous cases, like the ones studied in subsection 3.4. Repelling periodic nodes and expanding periodic saddles for this value of the parameter are also detected, and we note that the Lyapunov exponents of the attractor are both positive.

3.7. **The whole attractor.** Finally, in Figure 19f) the obtained attractor is shown for $t = 1.99999$. As was conjectured, see Conjecture 2, this situation would be frequently (with positive probability) observed for values of the parameter sufficiently close to $t = 2$: Almost all the invariant set R_2 is a 2D strange attractor with two positive Lyapunov exponents. For this particular value of the parameter the obtained exponents are 0.34491 and 0.34374, which are, as was also expected, very close to the value $\frac{1}{2}\log 2$, the (both) Lyapunov exponents for the bidimensional tent map studied in [21]. Furthermore, by making 10^3 equidistant experiments in the range of parameters $(1.99, 2)$ the shape of the obtained attractor always almost coincides with the whole domain R_2. This is not a proof of Conjecture 2 but gives a good support to it.

3.8. **Competition between coexisting attractors.** We end this section introducing Figure 20, where the distribution of sinks, invariant attracting curves, 1D and 2D strange attractors is shown. In the horizontal axis we select 1000 equidistant values for $t \in (1.886, 2)$. For each value of t, we also select 1000 equidistant initial conditions $(x_0, 0)$, with $x_0 \in [-4, 0]$. These values of x_0 are represented in the vertical axis of Figure 20. For each one of these critical points of T_t, the two Lyapunov exponents are calculated up to an error less than 10^{-4}. After this, each point (t, x_0) is coloured in Figure 20 according to the criterion used to depict Figure 2 (pale grey or blue, in the electronic version of the paper, for negative exponents, intermediate grey or green, for a zero Lyapunov exponent, dark grey or red, for 1D strange attractors and black for 2D strange attractors). We have taken in the figure the region

$$\{(t, x_0) \mid 1.886 < t < 2,\ -4 \le x_0 \le 0\}.$$

Therefore, different colors in the same vertical line in Figure 20 means the coexistence of different kinds of attractors for the respective value of t. This phenomenon

does not seem to be very frequent for our family of maps. On the other hand, we point out that the black region in the figure (2D strange attractors) prevails overall, as was expected, near the line $t = 2$. For the sake of completeness we also introduce Figure 21 where for $t \in (1.888, 1, 899)$, the competition between coexisting attractors is depicted. Namely, once a value of t is fixed we take the values $p_{po}, p_{ic}, p_{sa1}, p_{sa2} \in [0, 1]$ corresponding to the rate of values of x_0 (those taken in Figure 20) for which the orbit of the point $(x_0, 0)$ tends, respectively, to an attracting periodic orbit, an attracting invariant circle, a 1D strange attractor and a 2D strange attractor. Then, using the same colors than before, we draw a pale grey segment from $(t, 0)$ to (t, p_{po}), an intermediate grey segment from (t, p_{po}) to $(t, p_{po} + p_{ic})$ a dark grey segment from $(t, p_{po} + p_{ic})$ to $(t, p_{po} + p_{ic} + p_{sa1})$ and a black segment from $(t, p_{po} + p_{ic} + p_{sa1})$ to $(t, p_{po} + p_{ic} + p_{sa1} + p_{sa2})$. We remark that $p_{po} + p_{ic} + p_{sa1} + p_{sa2}$ is less than one, because for the first and the last values of x_0, the orbit of $(x_0, 0)$ does not converge to any attracting set. From this figure we see that the measure of values of (t, x_0) for which there are 2D strange attractors is very large, but there are significant zones in the depicted region for which there is coexistence of several kinds of attractors.

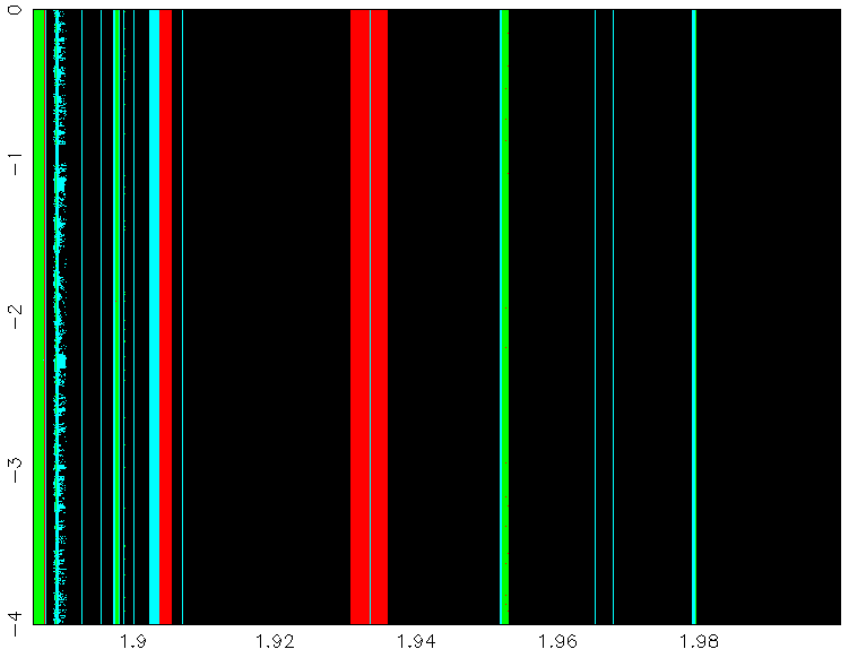

FIGURE 20. Coexistence of attractors for $t \in (1.886, 2)$. See explanations in the text.

4. **The whole family $T_{a,b}$ revisited.** All the numerical experiments shown along this paper were done on the curve G given in (4). Of course, at the sight of Figure 2 it

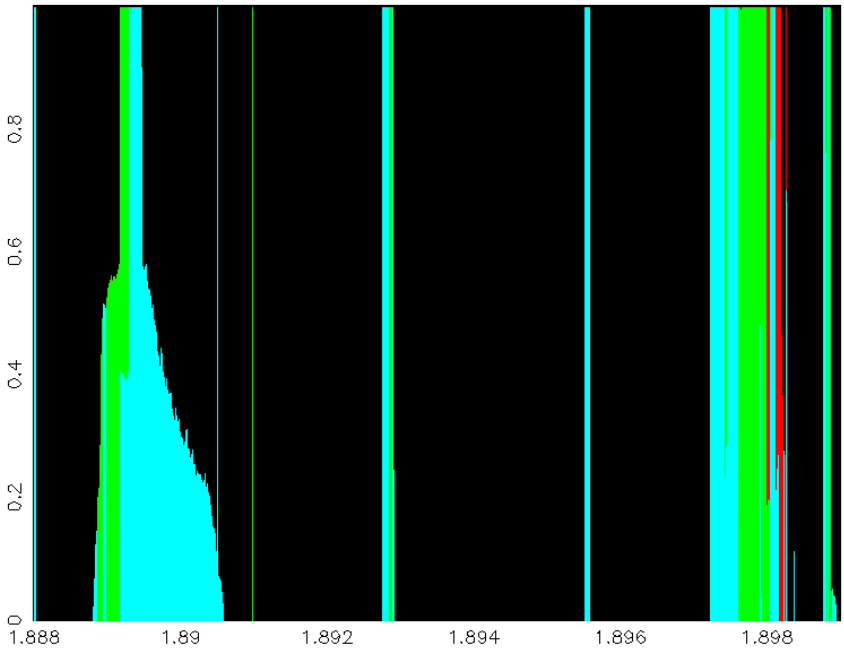

FIGURE 21. Proportion of different kinds of attractors for $t \in (1.888, 1, 899)$. See explanations in the text.

seems clear that similar behaviours may be found in different parts of the parameter space. For instance, we deem it wise to note that many Arnold's tongues appear (in pale gray) in the left hand side of the Hopf bifurcation line $2b - 4a = 3$. Hence, in order to study what happens in the nearness of such tongues it seems to be enough to consider just one of these tongues. We want to end this paper by giving some information about the behaviour of the whole family $T_{a,b}$. First we introduce Figure 22, where a magnification of some part of Figure 2 is presented. More concretely, by means of the same colour criterion used for Figure 2, we explore what kinds of attractors our map $T_{a,b}$ exhibits for $-1.25 \leq a \leq -0.5$, $0.25 \leq b \leq 0.75$. An Arnold's tongue can behave, in the proximity of the Hopf bifurcation line, as in the two-dimensional dissipative invertible maps case (see again [3]) where an attracting periodic orbit transforms finally into a 1D strange attractor. In our case, if we go beyond to the left, this attractor becomes a 2D strange attractor by some of the mechanisms we have described before. Namely, the process involves the existence of expanding saddles and repelling periodic orbits after some bifurcation (saddle-node or flip) and the behaviour of their unstable invariant manifolds. This seems to happen in the largest tongue in the picture. Another possibility for the behaviour of an Arnold tongue is that before the existence of a 1D strange attractor, a periodic point undergoes a Hopf bifurcation, what will give in a small scale a picture like the one obtained in Figure 22. Of course, the global behaviour of the map could be

very complicated as we saw in our family T_t , because several attractors can coexist. Finally, as we saw for T_t, it seems that near the line separating the region with attractors (in several tones of grey and black) and the region with no attractors (in white) the 2D strange attractors are more abundant than other kinds of attractors.

On the other hand, we can obtain some information about the border of the region B for which there are attracting sets, by computing some bifurcation curves. We begin by looking for codimension-two bifurcations of fixed points. As we have already pointed out, the Bogdanov-Takens bifurcation (where the eigenvalues of $DT_{a,b}$ at the fixed point are $\lambda_1 = \lambda_2 = 1$) corresponds to $(a, b) = \Gamma_1 = (1/4, 2)$. Also, it is easy to see that the bifurcation for which the eigenvalues are $\lambda_1 = -\lambda_2 = 1$ occurs for $(a, b) = \Gamma_2 = (1/4, 0)$, the bifurcation of resonance 1:2 ($\lambda_1 = \lambda_2 = -1$) for $(a, b) = \Gamma_3 = (-7/4, -2)$, and the bifurcation of resonance 1:3 ($\lambda_1 = \bar{\lambda}_2 = \exp(2\pi i/3)$), for $(a, b) = \Gamma_4 = (-5/4, -1)$. All these points seem to belong to the border of B (see Figure 23). Now if we compute codimension-one bifurcation curves associated to these codimension-two bifurcations, it seems that some of them are also in the border. The saddle-node bifurcation curve $\mathcal{C}_1$ has the equation $a = (b-1)^2/4$ and seems to match with the part of the border of B joining the points Γ_1 and Γ_2. The flip bifurcation curve $\mathcal{C}_2$ is given by the equation $a = -\frac{3}{4}b^2 - \frac{1}{2}b + \frac{1}{4}$ and apparently forms part of the border of B from the point Γ_2 to Γ_3. The curve corresponding to the heteroclinic connection arising at Γ_3 has the equation $b = -2$. Part of this curve at the left of Γ_3 (until the point $(-2, -2)$ where the heteroclinic connection disappears) seems to be in the border of B. Moreover, part of a curve of homoclinic tangency emerging at Γ_1 seems to lie on the border. Finally, part of a curve corresponding to a heteroclinic tangency appearing at Γ_4 apparently forms part of the border of B. We think that there are other codimension-two bifurcations which should help us to give a complete description of the border, including the homoclinic bifurcations present at $(a, b) = (-2, 0)$ and $(a, b) = (-4, -2)$. Notice, moreover, that at least part of the border of B has to exhibit a more complex structure due to the efect of the coexistence of several attractors in some parts of B, as we see in Figure 22. A more detailed study of these phenomena will be described elsewhere. In Figure 23 we have drawn part of the border of B jointly with some of the curves we have described along this section.

5. **Conclusions.** As was announced in the Introduction, we have put special emphasis along the paper in order to state the resemblances between our family of limit return maps, $T_{a,b}$, and the well-known quadratic family $Q_a(x) = 1 - ax^2$, which is the family of limit return maps prevailing for homoclinic phenomena for two dimensional diffeomorphisms ($m = 2$).

One must not forget that in [21] those resemblances were established between $T_{-4,-2}$ and Q_2, i.e., the final "Misiurewicz" limit return maps for the cases $m = 3$ and $m = 2$, respectively.

In fact, as we have observed in Section 3, many of these similarities arise when we restrict the study of $T_{a,b}$ to the curve G. Not only both families start with a fixed sink, but also all the known one dimensional classical bifurcations (saddle-node, period doubling cascade of bifurcations,...) were observed on G. Even Hopf bifurcations in dimension two have similarities with flip bifurcations in dimension one. Indeed, if we consider both bifurcations for fixed points, in the Hopf case we have an invariant set after the bifurcation which coincides with the border of a topological disk (the closed invariant curve), while in the flip case, the invariant

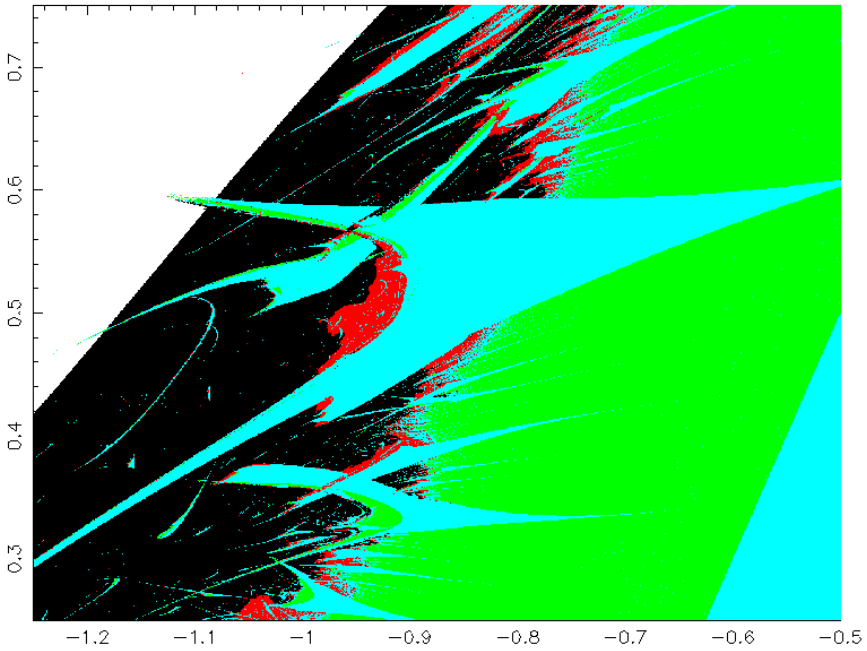

FIGURE 22. A magnification of Figure 2.

set is the border of an interval (formed by a periodic orbit of period two). The structure of many attractors arising in Section 3 matches with the one exhibited by the attractor corresponding to certain Q_a. For instance, attractors for $T_{a(t),b(t)}$, $(a(t), b(t)) \in G$, with several pieces containing a periodic repellor correspond to attractors for Q_a formed by the union of several disjoint intervals. Furthermore, the union of several pieces to give rise to a one-piece attractor is also a common phenomenon for the families Q_a and $T_{a(t),b(t)}$. These equivalences were explained along subsection 3.3, 3.4 and many others. Also the behaviour of the sum of the Lyapunov exponents function, see Figure 3.1, seems to be very similar to the one exhibited by the Lyapunov exponent function for Q_a. Hence, as expected, the attractors for both families for values of the parameters close enough to the respective "Misiurewicz" value, are completely equivalent: The whole invariant domain is a strange attractor for a positive Lebesgue measure set of parameters (recall that this is, so far, only a conjecture for our family $T_{a(t),b(t)}$). Beyond these "Misiurewicz" parameters there always exist critical points for both families whose orbit does not remain in a bounded region. Of course, in spite of the greater richness displayed by our family $T_{a(t),b(t)}$, we are convinced that these similarities will be crucial to develop a deeper study of the behaviour of $T_{a,b}$ starting by giving a positive answer to the open question introduced in Remark 1 and also to Conjectures 1 and 2 which, up to now, are only supported on numerical results.

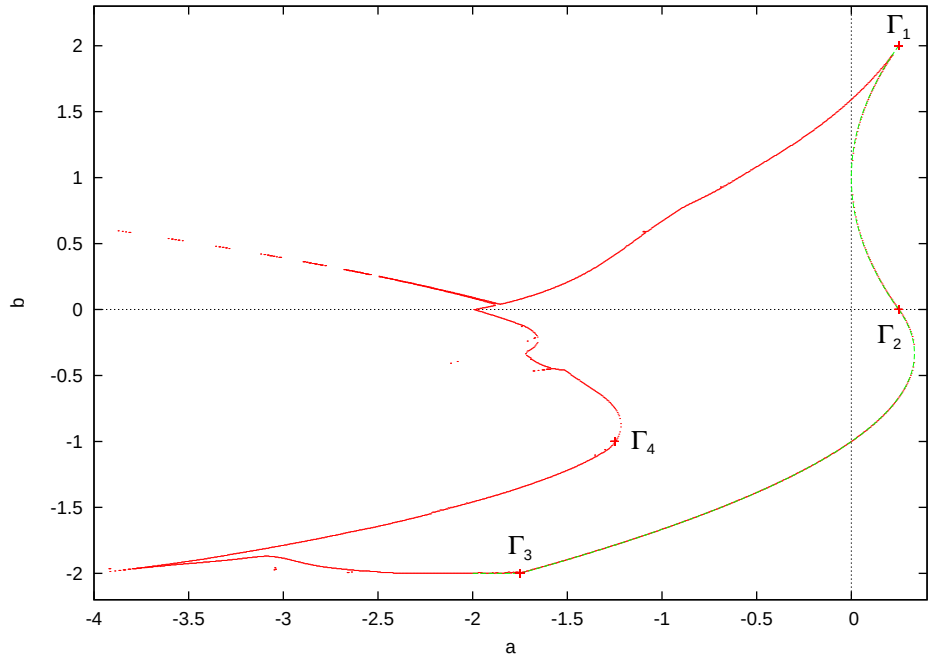

FIGURE 23. Border of the region of parameters for which there exist attracting sets. Coordinate axes are also drawn.

Finally, we want to insist in the relevance of the study of the map $T_{a,b}$ for the understanding of the behaviour of the attractors appearing near a generalized homoclinic tangency for a large class of three-dimensional dissipative diffeomorphisms because, as we said, $T_{a,b}$ is a limit return map for this kind of homoclinic bifurcation. Nevertheless, we cannot describe all the complexity of the geometry of the strange attractors, because what we see using our map can be considered as a projection in a subspace of dimension two of very complex objects in dimension three, specially in the case of 3D strange attractors.

Acknowledgements. We are indebted to C. Simó for fruitful discussions and suggestions. We are also very grateful for many contributions furnished by the anonymous referees.

REFERENCES

[1] M. Benedicks and L. Carleson, *On iterations of 1-ax^2 on* $(-1,1)$, Ann. Math., **122** (1985), 1-25.
[2] M. Benedicks and L. Carleson, *The dynamics of the Hénon map*, Ann. Math., **133** (1991), 73-169.
[3] H. Broer, C. Simó and J. C. Tatjer, *Towards global models near homoclinic tangencies of dissipative diffeomorphisms*, Nonlinearity, **11** (1998), 667-770.
[4] E. Colli, *Infinitely many coexisting strange attractors*, Ann. Inst. H. Poincaré, **15** (1998), 539-579.
[5] C. E. Frouzakis, L. Gardini, I. G. Kevrekidis, G. Millerioux and C. Mira, *On some properties of invariant sets of two-dimensional noninvertible maps*, Int. Jour. Bifur. and Chaos, **7** (1997), 1167-1194.

[6] C. E. Frouzakis, I. G. Kevrekidis and B. B. Peckham, *A route to computational chaos revisited: noninvertibility and the breakup of an invariant circle*, Physica D, **177** (2003), 101-121.
[7] S. V. Gonchenko, V. S. Gonchenko and J. C. Tatjer, *Bifurcations of three-Dimensional diffeomorphisms with non-simple quadratic homoclinic tangencies and generalized Hénon maps.* Regular and Chaotic Dynamics, **12** (2007), 233-266.
[8] M. Jacobson, *Absolutely continuous invariant measures for one parameter families of one-dimensional maps*, Commum. Math. Phys., **81** (1981), 39-88.
[9] J. L. Kaplan and J. A. Yorke, *Chaotic behavior of multidimensional difference equations*, Lecture Notes in Mathematics, **730** (1979), 204-227.
[10] Y. A. Kuznetsov, "Elements of Applied Bifurcation Theory", Springer-Verlag, New York, 1998.
[11] E. N. Lorenz, *Computational chaos-a prelude to computational instability*, Physica D, **35** (1989), 299-317.
[12] J. Milnor, *On the concept of attractor*, Commun. Math. Phys., **99** (1985), 177-195.
[13] C. Mira, L. Gardini, A. Barugola and J. C. Cathala, "Chaotic dynamics in two-dimensional noninvertible maps", World Scientific, Singapore, 1996.
[14] L. Mora and M. Viana, *Abundance of strange attractors*, Acta Mathematica, **171** (1993), 1-71.
[15] S. Newhouse, *Diffeomorphisms with infinitely many sinks*, Topology, **13** (1974), 9-18.
[16] J. Palis and F. Takens, "Hyperbolicity & sensitive chaotic dynamics at homoclinic bifurcations", Cambridge University Press, Cambridge, 1993.
[17] J. Palis and M. Viana, *High dimension diffeomorphisms displaying infinitely many sinks*, Ann. Math., **140** (1994), 91-136.
[18] H. Poincaré, *Sur le problème des trois corps et les équations de la dynamique (Mem. couronné du prix de S.M. le roi Oscar II de Suède).* Acta Math., **13** (1890), 1-270.
[19] A. Pumariño and J. A. Rodríguez, "Coexistence and persistence of strange attractors", Lecture Notes in Mathematics, **1658**, Springer, New York, 1997.
[20] A. Pumariño and J. A. Rodríguez, *Coexistence and persistence of infinitely many strange attractors*, Ergodic Theory and Dynamical Systems, **21** (2001), 1511-1523.
[21] A. Pumariño and J. C. Tatjer, *Dynamics near homoclinic bifurcations of three-dimensional dissipative diffeomorphisms*, Nonlinearity, **19** (2006), 2833-2852.
[22] R. Rico-Martínez, R. A. Adomaitis and I. G. Kevrekidis, *Non-invertibility in neutral networks*, Computers and Chemical Engineering, **24** (2000), 2417-2433.
[23] J. C. Tatjer and C. Simó. *Basins of attraction near homoclinic tangencies*, Ergodic Theory and Dynamical Systems, **14** (1994), 351-390.
[24] J. C. Tatjer, *Three-dimensional dissipative diffeomorphisms with homoclinic tangencies*, Ergodic Theory and Dynamical Systems, **21** (2001), 249-302.
[25] M. Viana, *Strange attractors in higher dimensions*, Bol. Soc. Bras. Mat. **24**, (1993), 13-62.

E-mail address: apv@uniovi.es
E-mail address: jcarles@maia.ub.es